



**HAL**  
open science

## **Time-limited alterations in cortical activity of a knock-in mouse model of KCNQ2 -related developmental and epileptic encephalopathy**

Najoua Biba-maazou, H el ene Becq, Emilie Pallesi-pocachard, Stefania Sarno, Samuel Granjeaud, Aur elie Montheil, Marie Kurz, Laurent Villard, Mathieu Milh, Pierre-pascal Lenck Santini, et al.

### **► To cite this version:**

Najoua Biba-maazou, H el ene Becq, Emilie Pallesi-pocachard, Stefania Sarno, Samuel Granjeaud, et al.. Time-limited alterations in cortical activity of a knock-in mouse model of KCNQ2 -related developmental and epileptic encephalopathy. *The Journal of Physiology*, inPress, 10.1113/JP282536 . hal-03654270

**HAL Id: hal-03654270**

**<https://amu.hal.science/hal-03654270>**

Submitted on 27 Jan 2023

**HAL** is a multi-disciplinary open access archive for the deposit and dissemination of scientific research documents, whether they are published or not. The documents may come from teaching and research institutions in France or abroad, or from public or private research centers.

L'archive ouverte pluridisciplinaire **HAL**, est destin ee au d ep ot et  a la diffusion de documents scientifiques de niveau recherche, publi es ou non,  emanant des  tablissements d'enseignement et de recherche fran ais ou  trangers, des laboratoires publics ou priv es.

# Time-limited alterations in cortical activity of a knock-in mouse model of *KCNQ2*-related developmental and epileptic encephalopathy

Najoua Biba-Maazou<sup>1</sup>, H el ene Becq<sup>1</sup>, Emilie Pallesi-Pocachard<sup>1</sup>, Stefania Sarno<sup>1</sup>, Samuel Granjeaud<sup>2</sup> , Aur elie Montheil<sup>1</sup>, Marie Kurz<sup>1</sup>, Laurent Villard<sup>3,4</sup>, Mathieu Milh<sup>3,5</sup>, Pierre-Pascal Lenck Santini<sup>1</sup> and Laurent Aniksztejn<sup>1</sup> 

<sup>1</sup>INSERM, INMED, Aix-Marseille University, Turing Centre for Living Systems, Marseille, France

<sup>2</sup>Centre de Recherche en Canc erologie de Marseille, INSERM, U1068, Institut Paoli Calmettes, CNRS, UMR7258, Aix-Marseille University UM 105, Marseille, France

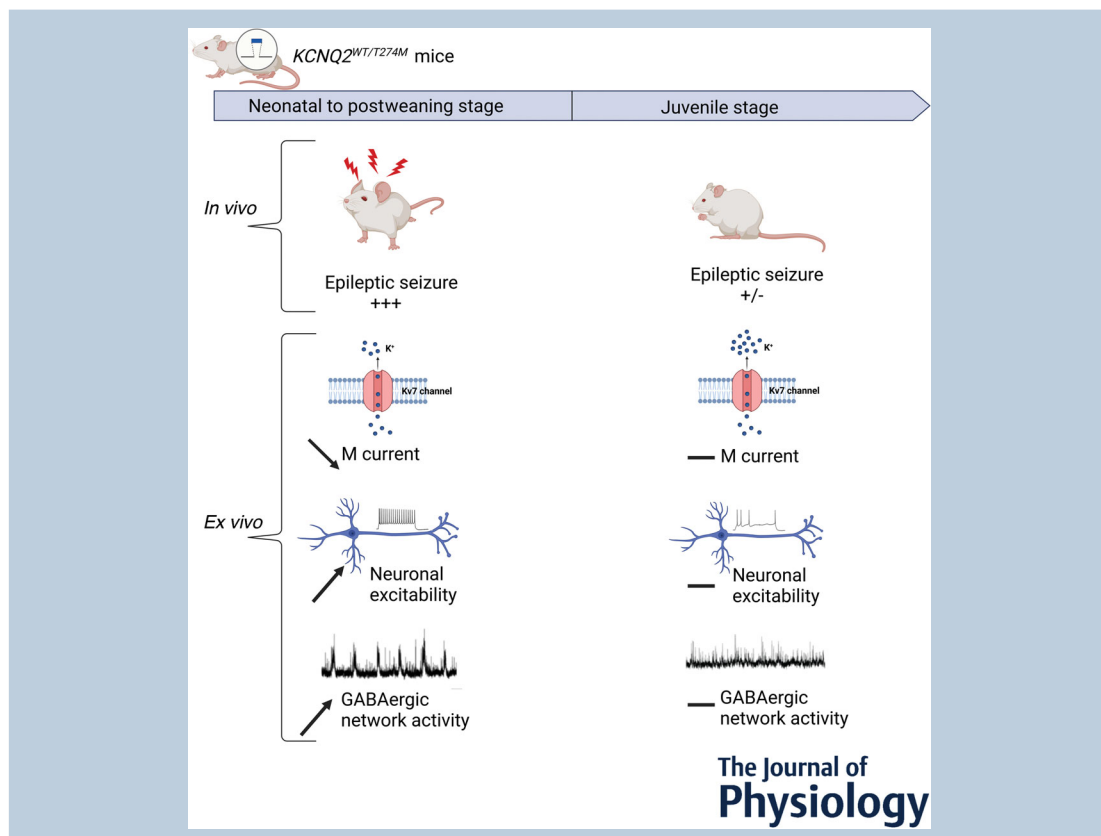
<sup>3</sup>Aix-Marseille University, INSERM, Marseille Medical Genetics Centre (MMG), Marseille, France

<sup>4</sup>Department of Medical Genetics, La Timone Children's Hospital, Marseille, France

<sup>5</sup>Department of Pediatric Neurology, La Timone Children's Hospital, Marseille, France

Edited by: David Wyllie & Jing-Ning Zhu

The peer review history is available in the Supporting information section of this article (<https://doi.org/10.1113/JP282536#support-information-section>).



[Correction added on June 10, 2022, after first online publication: The copyright line was changed.]

This article was first published as a preprint: Biba, N., Becq, H., Kurz, M., Pallesi, E., Villard, L., Milh, M., Lenck Santini, P. P., Aniksztejn, L. (2021). Time-limited alterations in cortical activity of a Knock-in mice model of *KCNQ2*-related Developmental and Epileptic Encephalopathy. *BioRxiv*. <https://doi.org/10.1101/2020.05.12.090464>

**Abstract** *De novo* missense variants in the *KCNQ2* gene encoding the Kv7.2 subunit of voltage-gated potassium Kv7/M channels are the main cause of developmental and epileptic encephalopathy with neonatal onset. Although seizures usually resolve during development, cognitive/motor deficits persist. To gain a better understanding of the cellular mechanisms underlying network dysfunction and their progression over time, we investigated *in vivo*, using local field potential recordings of freely moving animals, and *ex vivo* in layers II/III and V of motor cortical slices, using patch-clamp recordings, the electrophysiological properties of pyramidal cells from a heterozygous knock-in mouse model carrying the Kv7.2 p.T274M pathogenic variant during neonatal, postweaning and juvenile developmental stages. We found that knock-in mice displayed spontaneous seizures preferentially at postweaning rather than at juvenile stages. At the cellular level, the variant led to a reduction in M current density/conductance and to neuronal hyperexcitability. These alterations were observed during the neonatal period in pyramidal cells of layers II/III and during the postweaning stage in pyramidal cells of layer V. Moreover, there was an increase in the frequency of spontaneous network-driven events mediated by GABA receptors, suggesting that the excitability of interneurons was also increased. However, all these alterations were no longer observed in layers II/III and V of juvenile mice. Thus, our data indicate that the action of the variant is regulated developmentally. This raises the possibility that the age-related seizure remission observed in *KCNQ2*-related developmental and epileptic encephalopathy patients results from a time-limited alteration of Kv7 channel activity and neuronal excitability.

(Received 25 October 2021; accepted after revision 10 March 2022; first published online 7 April 2022)

**Corresponding author** Laurent Aniksztejn: INMED-INSERM UMR1249, Parc scientifique de Luminy, 163 route de Luminy, 13009 Marseille, France. Email: laurent.aniksztejn@inserm.fr

**Abstract figure legend** Knock-in mice harbouring the heterozygous pathogenic p.T274M variant in the Kv7.2 subunit (c.821C>T mutation of the *KCNQ2* gene) related to developmental and epileptic encephalopathy displayed epileptic seizures preferentially at postweaning rather than at juvenile developmental stages. At the cellular level, in motor cortical slices the variant led to a reduction in M current density, to a hyperexcitability of pyramidal cells and to an increase in the frequency of spontaneous network-driven events mediated by GABA receptors. All these alterations were time limited and were observed in pyramidal cells of neonatal mice until postweaning, but not of juvenile mice, in which the pyramidal cells had electrophysiological properties similar to those of wild-type mice.

### Key points

- The electrophysiological impact of the pathogenic c.821C>T mutation of the *KCNQ2* gene (p.T274M variant in Kv7.2 subunit) related to developmental and epileptic encephalopathy has been analysed both *in vivo* and *ex vivo* in layers II/III and V of motor cortical slices from a knock-in mouse model during development at neonatal, postweaning and juvenile stages.
- M current density and conductance are decreased and the excitability of layer II/III pyramidal cells is increased in slices from neonatal and postweaning knock-in mice but not from juvenile knock-in mice.
- M current and excitability of layer V pyramidal cells are impacted in knock-in mice only at the postweaning stage.
- Spontaneous GABAergic network-driven events can be recorded until the postweaning stage, and their frequency is increased in layers II/III of the knock-in mice.
- Knock-in mice display spontaneous seizures preferentially at postweaning rather than at juvenile stages.

## Introduction

Channelopathies represent one of the major causes of neurological disorders, including developmental and epileptic encephalopathy (DEE), a group of severe and intractable diseases, in which severe epilepsy is associated with an alteration of cognitive/sensory and motor functions. Among dozens of genes encoding for ion channels, *KCNQ2* is probably the one most frequently associated with DEE of neonatal onset (Allen et al., 2014, 2020; Dirkx et al., 2020; Kato et al., 2013; McTague et al., 2016; Milh et al., 2013; Weckhuysen et al., 2012; see also <http://www.rikee.org/>). *KCNQ2*-related DEE is characterized by seizures starting during the first days of life and often a highly abnormal EEG showing a suppression–burst pattern. As patients age, there is usually a positive evolution in terms of seizures and EEG abnormalities. However, despite seizure resolution, the neurological outcome remains poor, with severe motor and intellectual disabilities (Boets et al., 2021; Dirkx et al., 2020).

*KCNQ2* is one of the four genes identified in the CNS together with *KCNQ3–KCNQ5*, encoding the Kv7.2–Kv7.5 subunits, respectively, of the Kv7 channels (Jentsch, 2000). These subunits are abundant at the axon initial segment, nodes of Ranvier and synaptic terminals (Battefeld et al., 2014; Devaux et al., 2004; Huang & Trussell, 2011; Martinello et al., 2019; Shah et al., 2008). They are less expressed at the soma and absent in dendrites of cortical pyramidal cells, whereas in cortical interneurons they are detected in these subcellular regions (Lawrence et al., 2006).

Functional Kv7 channels are composed of homo- or heteromeric assemblies of four subunits including Kv7.2/Kv7.3 in many cortical neurons, giving rise to the M current (Battefeld et al., 2014; Brown & Passmore, 2009; Soh et al., 2014; Wang et al. 1998). The M current is a slowly activating and non-inactivating potassium current that activates at the subthreshold range of membrane potentials. The Kv7/M channels control different aspects of neuronal excitability (Adams et al., 1982; Greene & Hoshi, 2017; Jentsch, 2000; Storm, 1990), including the resting membrane potential at the axon initial segment and terminals, in addition to the spike threshold (Hu & Bean, 2018; Huang & Trussell, 2011; Martinello et al., 2019; Shah et al., 2008; Yue & Yaari,

2006). At nodes of Ranvier, Kv7 channels increase the availability of Na<sup>+</sup> channels, hence the amplitude of the propagating action potential (AP; Battefeld et al., 2014). At synaptic terminals, they can also control transmitter release (Huang & Trussell, 2011; Martinello et al., 2019; Vervaeke et al., 2006). Kv7 channels also reduce spike after-depolarization and, in some cells, mediate the medium after-hyperpolarization and contribute to the slow after-hyperpolarization (Gu et al., 2005; Kim et al., 2012; Storm, 1990; Yue & Yaari, 2006). Thus, Kv7 channels serve as a brake for neuronal firing. These channels also influence other aspects of neuronal function, such as the integration of excitatory postsynaptic potential in CA1 pyramidal cells (Hu et al., 2007; Shah et al., 2011) or the slow subthreshold resonance of cortical neurons at theta frequency (Hu et al., 2002).

Although the functional role of Kv7 channels and their different subunits is now well documented (Brown & Passmore, 2009; Fidzinski et al., 2015; Greene & Hoshi, 2017; Hou et al., 2021; Peters et al., 2005; Soh et al., 2014, 2018), the relationship between Kv7.2 variants and DEE remains poorly understood. The functional consequences of variants in the *KCNQ2* gene associated with DEE have been analysed widely in heterologous cells and, more recently, in patient induced pluripotent stem cell-derived neurons (Dirkx et al., 2020; Simkin et al., 2021). In heterologous cells, these studies have shown that most of the variants exerted a loss-of-function effect, reducing the M current carried by heteromeric channels from a moderate level (~25%) to a strong level (>50%) (Abidi et al., 2015; Allen et al., 2020; Miceli et al., 2013; Orhan et al., 2014; Simkin et al., 2021). This is notably the case for the p.T274M variant (c.821C>T in the *KCNQ2* gene). This variant exerts a dominant negative effect on the wild-type subunit, reducing current amplitude by 60% in a heterozygous configuration that mimics the situation in patients, without any effects on the conductance–voltage (*G–V*) relationship, protein production and membrane expression (Orhan et al., 2014). Recently, a knock-in (KI) mouse carrying the heterozygous p.T274M variant has been generated, the phenotype of which is reminiscent of some characteristics observed in *KCNQ2*-related DEE patients (Milh et al., 2020). In particular, spontaneous seizures have been recorded in juvenile KI mice, and cognitive impairment has been observed in adults. Thus, this KI mouse represents a good model to study

**Najoua Biba-Maazou** obtained a Master's degree at Aix-Marseille University (France) and is currently completing her PhD on the pathophysiological mechanisms of developmental and epileptic encephalopathy caused by a *KCNQ2*/Kv7.2 variant at the INMED-INSERM UMR 1249 institute (Aix-Marseille University).



how a Kv7.2 pathogenic variant alters cortical network functioning and, ultimately, help in designing therapeutic options.

In this study, we investigated, both *ex vivo* and *in vivo*, the electrophysiological consequences of the p.T274M pathogenic variant on cortical activity. We chose the neocortex to perform *ex vivo* electrophysiological recordings because most of the knowledge about DEE caused by *KCNQ2* variants comes from electrographic analysis of the neocortex. We focused our attention in the motor cortex because both *KCNQ2*-related DEE patients and heterozygous KI mice harbouring the p.T274M variant (*KCNQ2*<sup>WT/T274M</sup>) display tonic-clonic seizures that involve frontal structures (Milh et al., 2020). More precisely, we analysed in cortical slices the possible alterations that the variant might produce on pyramidal cell excitability, M current properties and spontaneous synaptic activities and performed a developmental study to see how these alterations, if any, evolved as animal aged from neonatal to juvenile stages. In addition, given that expression of ion channels might not be equivalent in pyramidal cells of the different cortical layers, we wondered whether the effect of the variant is the same or different between pyramidal cells of the layers II/III and V of the developing motor cortex. Finally, given that in patients, the frequency of seizures declines or remits during childhood (Boets et al., 2021), we wondered whether the occurrence of seizures is also regulated developmentally in these KI mice.

## Methods

### Animals and genotyping

All experiments were carried out in accordance with the European Communities Council Directive of 22 September 2010 (2010/63/UE) related to laboratory animals used for research purposes. The study was approved by the ethics committee of the 'Ministère de l'Enseignement Supérieur de la Recherche et de l'Innovation (APAFIS#27891-2020110514571312 v.2). Experiments were performed on male and female 129Sv mice from postnatal day (PND) 7 to PND 50, housed in a temperature-controlled environment with a 12 h–12 h light–dark cycle and free access to food and water (INMED animal facilities).

The generation of heterozygous *KCNQ2*<sup>WT/T274M</sup> KI mice and genotyping protocols were described by Milh et al. (2020). Briefly, mice were genotyped by PCR. The following two primers were included in the PCR: a common forward primer (5'-CTTGATCTTGTCCCCTGACTTGGTAGG-3') and a common reverse primer (5'-CCTAACATCTCCAGAGTAGGAAGGTGC G-3'). The primers amplified a 603 bp wild-type fragment and/or a 688 bp mutant fragment.

### Preparation of cortical slices

Experiments were performed on pyramidal neurons located in layers II/III and V of motor cortical slices.

Mice were decapitated after being killed by cervical dislocation. The brain was rapidly removed and placed in an oxygenated ice-cold choline solution containing (mM): 132.5 choline chloride, 2.5 KCl, 0.7 CaCl<sub>2</sub>, 3 MgCl<sub>2</sub>, 1.2 NaH<sub>2</sub>PO<sub>4</sub>, 25 NaHCO<sub>3</sub> and 8 glucose; oxygenated with 95% O<sub>2</sub> and 5% CO<sub>2</sub>. Coronal slices (300 μm thick) were cut using a vibratome (Leica VT1200S; Leica Microsystems, Germany) in ice-cold choline solution oxygenated with 95% O<sub>2</sub> and 5% CO<sub>2</sub>. Before recording, slices were incubated in an artificial cerebrospinal fluid solution of the following composition (mM): 125 NaCl, 3.5 KCl, 2 CaCl<sub>2</sub>, 1.3 MgCl<sub>2</sub>, 1.25 NaH<sub>2</sub>PO<sub>4</sub>, 26 NaHCO<sub>3</sub> and 10 glucose, equilibrated at pH 7.3–7.4 with 95% O<sub>2</sub> and 5% CO<sub>2</sub> at 34°C for 20 min, then at room temperature (22–25°C) for ≥1 h to allow recovery. Slices were placed into the recording chamber for electrophysiological purposes, where they were fully submerged and superfused with oxygenated artificial cerebrospinal fluid solution at 34–35°C at a rate of 5 ml/min.

### Ex vivo electrophysiology

Pyramidal cells of layers II/III and V were recorded under visual control with a Zeiss Axioscope 2FS microscope in cell-attached and whole-cell configurations using borosilicate glass capillaries (GC 150F-15). For recordings in current-clamp mode, patch pipettes were filled with a solution containing (mM): 140 KMeSO<sub>4</sub>, 6 NaCl, 10 Hepes, 1 MgCl<sub>2</sub>, 4 Mg-ATP and 0.4 Na<sub>2</sub>-GTP. The pH was adjusted to 7.35 with KOH. The resistance of the pipettes was 5–6 MΩ. For recordings of spontaneous synaptic activities in voltage-clamp mode, patch pipettes were filled with a solution containing (mM): 120 caesium gluconate, 10 CsCl, 10 Hepes, 4 Mg-ATP and 0.4 Na<sub>2</sub>-GTP. The pH was adjusted to 7.35 with CsOH. The resistance of the pipettes was 6–7 MΩ. For recordings of M current, patch pipettes were filled with a solution containing (mM): 135 potassium gluconate, 10 KCl, 10 Hepes, 5 phosphocreatine, 4 Mg-ATP and 0.4 Na<sub>2</sub>-GTP. The pH was adjusted to pH 7.35 with KOH. The resistance of the pipettes was of 5–7 MΩ.

All reported potential values were corrected for the liquid junction potential, calculated to be ~2 mV with the KMeSO<sub>4</sub> pipette solution and ~15 mV with the caesium gluconate and potassium gluconate pipette solutions.

Recordings in current-clamp mode were performed in the presence of 2,3-dioxo-6-nitro-1,2,3,4-tetrahydrobenzo[*f*]quinoxaline-7-sulfonamide (NBQX, 10 μM) to block AMPA/kainate receptors; D-2-amino-5-phosphonovalerate (D-APV, 40 μM) to block

NMDA receptors; 6-imino-3-(4-methoxyphenyl)-1(6H)-pyridazinebutanoic acid hydrobromide (SR 95531, gabazine 5  $\mu\text{M}$ ) to block GABA<sub>A</sub> receptors. Some experiments were performed in the continuous presence of the Kv7 channel blocker 10,10-bis(4-pyridinylmethyl)-9(10H)-anthracenone dihydrochloride (XE-991, 20  $\mu\text{M}$ ). In these slices, pyramidal cell recordings were performed ~20–30 min after starting the superfusion with XE-991 (see Hu & Bean, 2018). All these drugs were purchased from Tocris Bioscience (Bristol, UK).

The resting membrane potential was determined in current-clamp mode as the potential upon break-in, before any current injection. The AP threshold was defined as the membrane potential at which the rate of depolarization is maximal. All measurements were filtered at 3 kHz using an EPC10 amplifier (HEKA Elektronik, Germany) and sampled at 10 kHz. Data were analysed off-line using Clampfit (Molecular Devices), miniAnalysis (Synaptosoft), Origin 9 (Origin Lab) and Prism 6 software (GraphPad).

Only cells with a stable resting membrane potential more negative than  $-60$  mV were used. All measurements in current-clamp mode were performed from a membrane potential of  $-70$  mV ( $-72$  mV with liquid junction potential correction) and, if necessary, current was injected during the experiment to keep this value constant.

To calculate the membrane input resistance ( $R_m$ ), voltage responses to the injection of five depolarizing and hyperpolarizing current steps, with an increment of  $\pm 5$  pA and applied for 500 ms, were fitted with a linear function to yield the slope value.

To calculate the membrane time constant ( $\tau_m$ ), the voltage response to the injection of a hyperpolarizing current step of  $-20$  pA for 500 ms was fitted with a single exponential function (Origin 9) to yield  $\tau_m$ . Membrane capacitance ( $C_m$ ) was then calculated according to the equation:  $C_m = \tau_m/R_m$ .

Action potentials were elicited by injection of short (10 ms) and long (1 s) depolarizing current steps of 20–300 pA (in 20 pA increments) in pyramidal cells from animals aged 1 week and steps of 50–750 pA (in 50 pA increments) from older animals. Currents injected by a slow ramp protocol were of 300 and 500 pA applied for 10 s in pyramidal cells from animals aged 1 week and from older animals, respectively.

The M current was recorded in the presence of NBQX (10  $\mu\text{M}$ ), D-APV (40  $\mu\text{M}$ ), SR 95531 (5  $\mu\text{M}$ ), tetrodotoxin (TTX, 1  $\mu\text{M}$ ) to block voltage-gated Na<sup>+</sup> channels, CsCl (2 mM) to block the Na<sup>+</sup>/K<sup>+</sup> HCN/ $I_H$  channels, 4-aminopyridine (4-AP, 2 mM) to block the fast activating/ slow inactivating voltage-gated potassium Kv1/ $I_D$  channels and the fast activating/fast inactivating voltage-gated potassium Kv4/ $I_A$  channels and CdCl (200  $\mu\text{M}$ ) to block voltage-gated Ca<sup>2+</sup> channels and calcium-dependent potassium channels.

In order to activate Kv7 channels, a slow ramp of voltage was applied from  $-90$  mV to reach  $+10$  mV in 30 s. Cells were maintained for 1 s at this membrane potential, and 1 s hyperpolarizing voltage steps down to  $-90$  mV (in 10 mV increments) were applied to deactivate the channels. A short (100 ms) hyperpolarizing voltage step command of 10 mV was applied at  $-90$  mV before each slow ramp of voltage to ensure the stability of the access resistance and the quality of the recordings (Fig. 5A). The M current amplitude was measured as the difference between the instantaneous ( $I_{\text{ins}}$ ) and steady-state current ( $I_{\text{ss}}$ ) levels at the onset and end of each hyperpolarizing voltage step applied from  $+10$  mV, respectively (Fig. 5D and E). The conductance ( $G$ ) values were obtained from the deactivated current amplitude divided by the driving force for K<sup>+</sup> [ $G = I/V - E_K$ , where  $V$  is the membrane potential at which the current was measured and  $E_K$  is the reversal potential for K<sup>+</sup> ions calculated by the Nernst equation ( $\sim -94$  mV in our recording conditions)].

To measure the current deactivation kinetics, current traces were fitted with a single or double exponential function of the following form:  $y = A_{\text{fast}}\exp(-\tau/\tau_{\text{fast}}) + A_{\text{slow}}\exp(-\tau/\tau_{\text{slow}})$ , where  $A_{\text{fast}}$  and  $A_{\text{slow}}$  are the fractions of the fast and slow components of the current and  $\tau_{\text{fast}}$  and  $\tau_{\text{slow}}$  are the respective fast and slow time constants. The time constant representing the weighted average of the fast and slow components of current deactivation was calculated with the following equation:  $\tau = (\tau_{\text{fast}}A_{\text{fast}} + \tau_{\text{slow}}A_{\text{slow}})/(A_{\text{fast}} + A_{\text{slow}})$ . Currents were analysed using Origin 9.0 software.

### In vivo video and EEG monitoring

For ethical reasons, we performed video and EEG monitoring for a maximum of 48 h after weaning. Tethered recordings would require isolating the pups from the dam before weaning, and radio-telemetry devices are too large for implantation in animals younger than PND 60. For these reasons, recordings were performed starting from postweaning age (PND 18–20) and using custom-made tether-pre-amplifier assemblies allowing the mice to move freely. The recording apparatus was adapted by the manufacturer (Neuralynx, Bozeman, MT, USA). It consisted of a 64-channel Digitalynx SX (24 bit A/D converter) connected to a four-way cable splitter. Each input cable was connected to a 16-channel headstage pre-amplifier that allowed the recording of signals from up to four freely moving mice at a time. An ethernet camera (Basler acA1300-75gc) was placed above the cages and connected to a Gigabit ethernet acquisition card (Neuralynx). The recording software interface (Cheetah v.6.4.1) allowed the simultaneous recording of intracranial local field potentials from all mice synchronously with the video signal from the camera. Local field potentials

(recorded against the earth) and video data were acquired at 1 kHz and 30 Hz, respectively.

Electrode arrays consisted of four 50  $\mu\text{m}$  nichrome, formvar-insulated wires bent and cut to the desired lengths. A 76  $\mu\text{m}$  stainless-steel wire (A-M system) serving as an earth lead was bent perpendicularly and cut at 1.5 mm. During surgery, the tip of this wire was de-insulated for 1 mm. All wires were connected to a board-to-board connector (Mill-Max Manufacturing).

## Surgery

Thirty minutes before surgery, mice were anaesthetized with 4% isoflurane and injected with buprenorphine s.c. (Buprecare, 0.03 mg/kg). They were then re-anaesthetized (4% isoflurane for induction, decreased progressively to 1.5% for maintenance of anaesthesia), placed in the stereotaxic apparatus (Kopf Instruments) and breathing through an anaesthesia mask (TEM Segal, France). The scalp was shaved and cleaned with three successive treatments of betadine and 70% ethanol. Body temperature was maintained at 36°C throughout the procedure with a heating pad placed underneath the animal and monitored with a rectal probe (FHC). An ophthalmic gel was placed on the eyes (lanolin and retinol mix, Vitamin A Dulcis, France) to prevent dryness. Lidocaine 5% was injected s.c. under the scalp, 5 min before incision. The scalp was then removed and the bone surface cleaned. Small incisions were made into the bone surface, and holes were drilled at the following coordinates (in millimetres with respect to bregma): at PND 18–20: prefrontal cortex (PFC), anteroposterior = +0.1, lateral =  $\pm 0.09$  and dorsoventral = 1.5; and hippocampus, anteroposterior = -0.23, lateral =  $\pm 0.25$  and dorsoventral = 2.5; and at PND 34–50: PFC, anteroposterior = +0.12, lateral =  $\pm 0.12$  and dorsoventral = 1.5; and hippocampus, anteroposterior = -0.23; lateral =  $\pm 0.27$  and dorsoventral = 2.5.

Recordings were performed in the PFC and the hippocampus rather than in the motor cortex. In rodents, the motor area is close to bregma and localized at the level of the coronal suture, where the vasculature is important, which makes electrode implantation hazardous. The recording electrode was therefore placed in a safer position in front of the coronal suture, reaching the PFC in close proximity of the motor cortex. Owing to volume conduction, it is likely that any seizures generated in the motor cortex will be observed in the PFC.

Electrode wires were bent by 90° 1 mm before the tip and inserted through the craniotomies. The earth wire was placed above the cerebellum, through a hole in the dorsal skull suture. Veterinary-grade cyanoacrylate gel (Vetbond, 3M) was used to secure electrodes on the skull and spread throughout the skull. Dental cement (Paladur, Kulzer) was then used to secure the body of the implant to the skull.

## Video and EEG monitoring

On the day of recordings, up to four postweaning (PND 18–20) or adult (PND 34–50) mice were connected to the cable-headstage assembly. They were allowed to move freely in their home cage (one animal per cage, 33.2 cm  $\times$  15 cm  $\times$  13 cm) and had access to standard food diet and non-wetting water gel for hydration (Hydrogel, ClearH2O, Westbrook, ME, USA). Recordings were started in the afternoon after surgery. Animals were inspected regularly during the day (every 2 h) to ensure that they did not have any adverse reactions to the surgery and recording procedure. To keep recordings to a reasonable size, a Matlab (Mathworks, MA, USA) routine was used for remote control of the Cheetah acquisition software (Neuralynx) and started a new recording every half hour.

Mice were killed at the end of the 48 h of video and EEG recordings using isoflurane anaesthesia (5%) followed by cervical dislocation. The brain was removed and cut to verify the position of the electrodes.

## Data analysis

Data analysis was performed using custom-made Matlab routines and graphical user interfaces. The local field potential signal was bandpass filtered (1–400 Hz), and putative interictal spikes were detected automatically using the method of White et al. (2006). Briefly, an interictal spike was considered each time the slope of the signal over 16 ms was greater than six times the standard deviation and its amplitude was greater than three times the standard deviation of the local field potential. Putative interictal spikes were then visualized together with the corresponding video. Scratching, chewing or bumping artefacts were therefore detected and removed from analysis. Other types of electrical artefacts, characterized by vertical slopes and symmetrical shapes, were also discarded. Seizures were considered when >20 interictal spikes were detected in a 10 s window.

## Western blot

Mice (PND 7, PND 21 and PND 30) were killed by cervical dislocation and decapitated. The brains were quickly removed and placed in choline chloride solution at 4°C. Coronal slices (300  $\mu\text{m}$ ) were prepared. Different parts of the motor cortex were separated [superficial layers (layers I and II/III) and deep layers (layer V/VI)]. Tissues were sonicated and the cells dissociated (26-gauge syringe) and lysed in RIPA buffer solution (ThermoFisher Scientific) supplemented with protease and phosphatase inhibitor cocktail (ThermoFisher Scientific) according to the manufacturer's protocol. The protein concentration

was determined using the BCA assay (Thermo Fisher Scientific) according to the manufacturer's protocol. Total proteins (75  $\mu\text{g}$ ) were heat-denatured, processed by SDS-PAGE and transferred to a nitrocellulose blotting membrane according to the manufacturer's protocol of the fast Pierce Blotter (ThermoFisher Scientific). Each membrane was cut in two slightly below the 70 kDa size marker to reveal proteins of interest with a molecular weight higher than our reference protein, glyceraldehyde 3-phosphate dehydrogenase (GAPDH; 37 kDa). After blotting with primary antibodies [rabbit anti-KCNQ2 (1:1000) and anti-KCNQ3 (1:1000), both kindly gifted by Dr Jérôme Devaux (see Abidi et al., 2015; Devaux et al. 2017) and GAPDH (1:2000; PA1-987; ThermoFisher Scientific)] and secondary HRP conjugate antibody, the substrate HRP Immobilon Western reagent (Merck Millipore) was used for signal detection according to the manufacturer's instructions. GAPDH was used as the internal control for normalization of the intensity of Kv7.2 and Kv7.3 bands.

### Statistical methods

Data shown in graphs are represented as the mean  $\pm$  SD. Student's unpaired *t* test was used to compare the means of two groups when the data distribution was normal. When the normality test failed, we used the non-parametric Mann-Whitney *U* test for two independent samples. The normality was assessed using the Shapiro-Wilk test. Those statistical analyses were performed using GraphPad Prism v.9 software. To evaluate the difference between two groups of curves statistically (Figs 1, 3, 6 and 7), we applied a non-parametric two-way ANOVA with repeated measures (two-way RM-ANOVA), in which the responses (*y*-axis) from the same cell across the discrete values of the *x*-axis were taken as repeated measurements. Given that some data were not normally distributed and equally variable, we took the non-parametric approach available in the package nparLD 2.1 (non-parametric longitudinal data) in R v.3.6.3. We applied the Benjamini-Hochberg correction after the non-parametric RM-ANOVA when three groups of curves were compared (Figs 1 and 3). We used a one-way ANOVA with Tukey's correction or the Kruskal-Wallis test with Dunn's correction for multiple comparisons when data of three independent groups were compared (Figs 2 and 4). Statistical significance was considered at  $P < 0.05$  for all tests. For better readability, *P*-values are indicated in the figures only when there is a significant difference. Values and statistical tests used are indicated in the statistical summary table.

### Results

Pyramidal cells located in layers II/III and V of the developing motor cortex were recorded using the

patch-clamp technique in slices from mice aged 1 week (neonatal, PND 7–9), 3 weeks (postweaning, PND 19–21) and 4–5 weeks (juvenile, PND 28–35).

The properties of the cells obtained from wild-type mice (*KCNQ2*<sup>WT/WT</sup>, hereafter referred to as 'wild-type cells') and from *KCNQ2*<sup>WT/T274M</sup> mice (hereafter referred to as 'mutant cells') were compared. Furthermore, given that the p.T274M variant exerts a loss-of-function effect on Kv7/M channel activity in heterologous systems (Orhan et al., 2014), we also analysed the action of the potent Kv7/M channel blocker XE-991 (20  $\mu\text{M}$ ) on pyramidal cell properties of wild-type mice to determine whether the variant and the blocker had similar electrophysiological consequences. For this purpose, slices obtained from *KCNQ2*<sup>WT/WT</sup> mice were superfused with the blocker (*KCNQ2*<sup>WT/WT</sup> in XE-991, hereafter referred to as 'XE-991-treated wild-type cells').

### The p.T274M variant transiently increases the excitability of pyramidal cells of layers II/III

At PND 7–9, in cell-attached configuration, pyramidal cells of layers II/III recorded in the three groups of slices were silent; there was no spontaneous discharge in wild-type cells recorded in either the absence or the presence of XE-991, nor in mutant cells ( $n = 17$  wild-type cells from two animals;  $n = 11$  XE-991-treated wild-type cells from two animals;  $n = 17$  mutant cells from three animals; Fig. 1Aa), indicating that the variant did not excite pyramidal cells at their resting membrane potential. In whole-cell configuration, compared with wild-type cells, mutant cells and XE-991-treated wild-type cells exhibited a higher  $R_m$ , a lower current threshold (rheobase) to elicit a single AP by short 10 ms depolarizing current steps and a more hyperpolarized AP membrane threshold (Table 1).

We then analysed the neuronal discharge elicited by the injection of depolarizing current steps from 20 to 300 pA during 1 s. We quantified the number of APs and the frequency of discharge during the first 200 ms of the steps (initial frequency) and during the last 200 ms of the steps (final frequency). The presence of the variant or treatment with the M channel blocker led to a large and significant leftward shift of the relationship between the number of APs and the amplitude of the current injected up to a current step of 160 pA (#AP-*I*; Fig. 1Ab and Ac). For current steps of larger amplitude, the #AP-*I* relationship reached a plateau, and the number of APs even decreased in XE-991-treated wild-type cells (Fig. 1Ab and Ac). The initial and final frequencies of the discharge were also affected by the variant and the treatment with XE-991. A significant leftward shift of the initial frequency-current (*iF*-*I*) relationship was observed for the two groups of cells, in addition to the final frequency-current (*fF*-*I*)

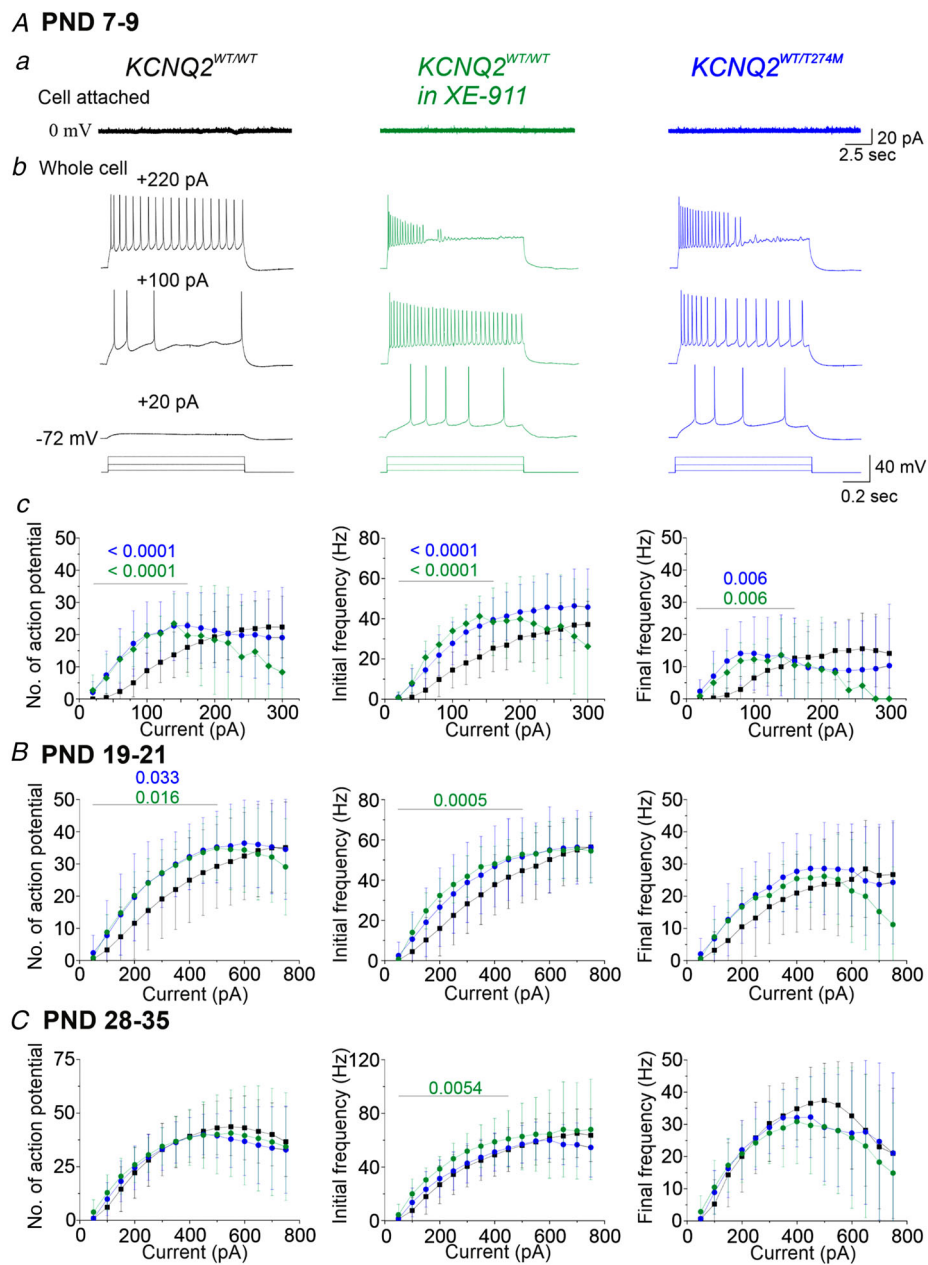


**Figure 1. Effects of XE-991 and of the p.T274M variant on the discharge of developing layers II/III pyramidal cells elicited by injection of current steps**

**Aa**, representative traces showing recordings of pyramidal cells in the cell-attached configuration in motor cortical slices from a *KCNQ2*<sup>WT/WT</sup> mouse (left traces, black), from a *KCNQ2*<sup>WT/WT</sup> mouse superfused with 20  $\mu$ M XE-991 (middle traces, green) and from a *KCNQ2*<sup>WT/T274M</sup> mouse (left trace, blue), all aged 1 week [postnatal day (PND) 7–9]. **Ab**, same cells recorded in the whole-cell configuration, showing voltage responses to the injection of three depolarizing current steps of 20, 100 and 220 pA applied during 1 s. **Ac**, graphs quantifying (mean  $\pm$  SD), at PND 7–9, the number of action potentials elicited by the injection of depolarizing current steps (left graph), the initial frequency (measured during the first 200 ms of the steps, middle graph) and the final frequency (measured during the last 200 ms of the steps, right graph) of the discharge. Black, wild-type cells ( $n = 17$  cells from two animals); green, XE-991-treated wild-type cells ( $n = 11$  cells from two animals); and blue, mutant cells ( $n = 17$  cells from three animals). **B**, same quantifications as in **Ac** in cells from mice aged 3 weeks (PND 19–21). Black, wild-type cells ( $n = 20$  cells from four animals); green, XE-991-treated wild-type cells ( $n = 21$  cells from four

The Journal of  
Physiology

animals); and blue, mutant cells ( $n = 22$  cells from four animals). C, same quantification of the three parameters in cells from mice aged 4–5 weeks (PND 28–35). Black, wild-type cells ( $n = 27$  cells from five animals); green, XE-991-treated wild-type cells ( $n = 25$  cells from five animals); and blue, mutant cells ( $n = 25$  cells from four animals). Statistical comparisons (two-way repeated-measures ANOVA with Benjamini–Hochberg correction for multiple comparisons) were made on measurements from the starting point of the curve (for an injected current of 20 or 50 pA) to saturation of the response at each developmental stage. The  $P$ -values are indicated when there is a significant statistical difference. The  $P$ -values are also given in the statistical summary table. Green, *KCNQ2*<sup>WT/WT</sup> (wild-type cells) vs. *KCNQ2*<sup>WT/WT</sup> in XE-991 (XE-991-treated wild-type cells); blue, *KCNQ2*<sup>WT/WT</sup> (wild-type cells) vs. *KCNQ2*<sup>WT/T274M</sup> (mutant cells); and black, XE-991-treated wild-type cells vs. mutant cells. Underlying numerical values can be found in the statistical summary table (for  $A_C$ , number of action potentials, to C, final frequency).

relationship for current steps  $\leq 160$  pA (Fig. 1Ac). The decrease in the number and frequency of APs in mutant and XE-991-treated wild-type cells for current steps of strong amplitude was probably a consequence of the high input resistance of these two groups of cells leading to a much larger depolarization and to the progressive inactivation of voltage-gated Na<sup>+</sup> channels.

We next examined the membrane response of the same cells to the injection of a slow ramp of current of 300 pA applied over 10 s. This procedure should reveal much better the action of Kv7 channels, which do not present voltage- and time-dependent inactivation, unlike many other ion channels. Several parameters of the response were analysed. These included the resistance of the ramp measured between  $-72$  mV and the AP threshold ( $R_{\text{ramp}}$ ), the current required to evoke the first AP ( $I_{\text{threshold}}$ ), the number of APs, the initial frequency during the first 200 ms of the discharge and the variation of voltage produced by the ramp. Most of these parameters were significantly affected in the same direction by the variant or after inhibition of Kv7 channels (Fig. 2A). In comparison to wild-type cells ( $n = 16$ ), the current threshold of both mutant cells ( $n = 17$ ) and XE-991-treated wild-type cells ( $n = 11$ ) was decreased, the AP membrane threshold was more hyperpolarized (only for XE-991-treated cells), the initial frequency of the discharge was increased, and the variation of voltage was more important in both XE-991-treated wild-type cells and mutant cells with similar mean values, although a statistical difference was observed only for mutant cells.

Therefore, at the end of the first postnatal week of life, the variant or the inhibition of M channels had the same consequences for the electrophysiological properties of layers II/III pyramidal cells; both made cells more excitable in response to the injection of steps or a ramp of current. However, neither the p.T274M variant nor XE-991 rendered cells spontaneously more excited.

At PND 19–21, wild-type pyramidal cells ( $n = 20$  cells from four animals) had higher capacitance, half input resistance and a faster membrane time constant than at PND 7–9 (Table 1). Moreover, the current threshold to elicit an AP by the injection of steps or a ramp of current was higher (Figs 1B and 2B). Most of the effects of the variant and of XE-991 described at PND 7–9 on membrane responses to current injection were maintained

at 3 weeks. As at PND 7–9, in cell-attached configuration, the variant or treatment with the blocker did not lead pyramidal cells to fire APs spontaneously ( $n = 22$  mutant cells from four animals and 21 XE-991-treated wild-type cells from four animals; data not shown). In whole-cell configuration, the responses of the cells to the injection of steps (50–750 pA) or a ramp of current (500 pA in 10 s) were increased to a similar extent compared with the responses of wild-type cells (Figs 1B and 2B), although the leftward shift of the  $iF$ – $I$  relationship observed in mutant cells was not significantly different (Fig. 1B). The excitability of pyramidal cells in the mutant and XE-991-treated wild-type cells was significantly enhanced in comparison to wild-type cells and observed for a wider range of current injected at PND 7–9.

At PND 28–35, the response of wild-type pyramidal cells to current steps but not to the injection of a slow ramp of current was stronger than at PND 19–21 (Figs 1C and 2C). The #AP– $I$ ,  $iF$ – $I$  and  $fF$ – $I$  relationships were steeper at PND 28–35 ( $n = 27$  wild-type cells from five animals; Fig. 1C). The presence of the variant affected neither the discharge of the AP elicited by the injection of current steps nor the response of the cells to the injection of a slow ramp of current ( $n = 25$  mutant cells from four animals). In contrast, XE-991 ( $n = 25$  cells from five animals) produced a significant leftward shift of the  $iF$ – $I$  relationship, while the #APs was increased for current steps  $\leq 200$  pA ( $P = 0.024$ ; Fig. 1C), and significantly affected in the same way as at PND 19–21 some of the parameters of the membrane response to the injection of a slow ramp of current (Fig. 2C).

Therefore, the increase in pyramidal cell excitability produced by the variant was limited to the first 3 weeks of postnatal life, whereas the electrophysiological alterations produced by XE-991 were maintained from neonatal to juvenile stages at least.

### Layer V pyramidal cells are impacted at a later developmental stage by the variant than in layers II/III but also transiently

We next wondered whether the variant and XE-991 impacted the excitability of pyramidal cells of other layers of the motor cortex and whether these cells presented the same developmental sensitivity as described above

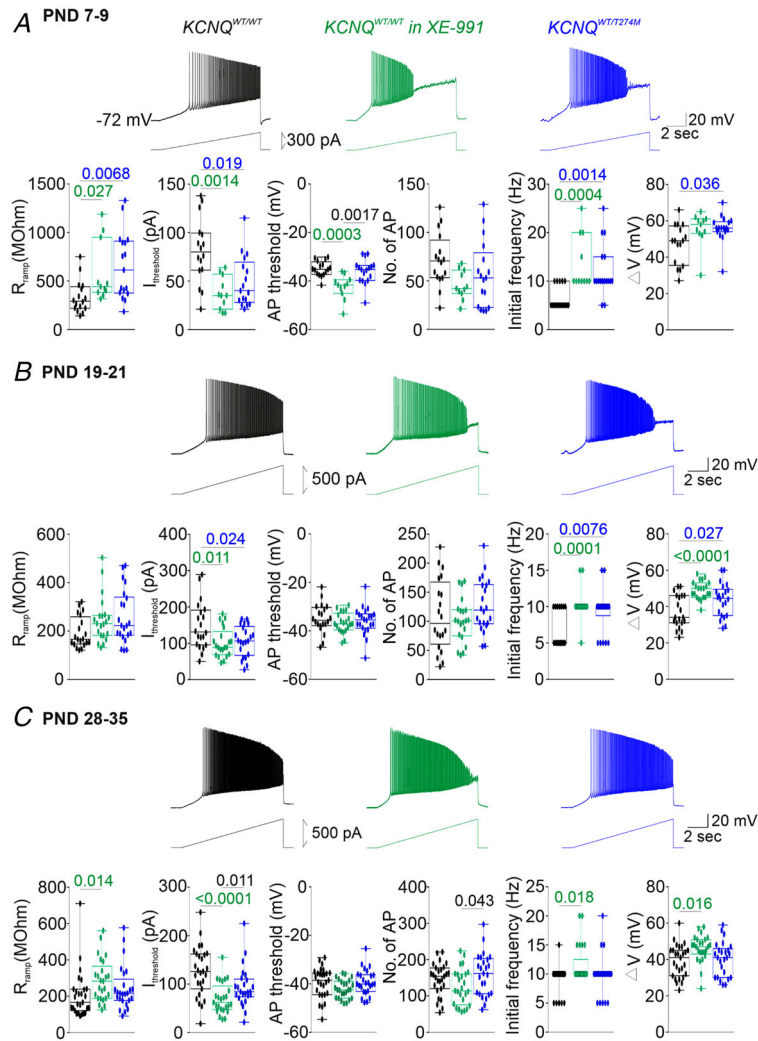
**Table 1.** Intrinsic properties of pyramidal cells of layers II/III in motor cortical slices from *KCNQ2*<sup>WT/WT</sup> mice (black), *KCNQ2*<sup>WT/WT</sup> mice superfused with XE-991 (20 μM, green) and *KCNQ2*<sup>WT/WT274M</sup> mice (blue) aged 1, 3 and 4–5 weeks

Layers II/III	PND 7–9 <i>KCNQ2</i> <sup>WT/WT</sup> <i>KCNQ2</i> <sup>WT/WT</sup> in XE-991 <i>KCNQ2</i> <sup>WT/WT274M</sup>	PND 19–21 <i>KCNQ2</i> <sup>WT/WT</sup> <i>KCNQ2</i> <sup>WT/WT</sup> in XE-991 <i>KCNQ2</i> <sup>WT/WT274M</sup>	PND 28–35 <i>KCNQ2</i> <sup>WT/WT</sup> <i>KCNQ2</i> <sup>WT/WT</sup> in XE-991 <i>KCNQ2</i> <sup>WT/WT274M</sup>
	<i>C<sub>m</sub></i> (pF)	67.6 (21.9) 59.0 (12.4) 59.3 (27.8)	92.5 (28.2) 112.7 (25.3) 101.9 (36.6)
<i>V<sub>m</sub></i> (mV)	−65.9 (3.6) −67.8 (4.2) −66.3 (5.4)	−69.9 (4.3) −68.9 (5.5) −72.3 (5.1)	−73.7 (7.1) −70.2 (6.1) −73.4 (3.3)
<i>R<sub>m</sub></i> (mΩ)	324.2 (100.4) 483.5 (109.7)* 560.0 (220.3)*** (One-way ANOVA <i>P</i> = 0.034) (One-way ANOVA <i>P</i> = 0.0003)	169.2 (63.9) 203.3 (56.6) 202.7 (96.0)	157.8 (78.7) 229.3 (96.2)* 185.6 (90.3) (K-W <i>P</i> = 0.013)
<i>τ<sub>m</sub></i> (ms)	25.6 (7.2) 26.7 (9.6) 26.5 (9.7)	17.2 (4.7) 21.1 (6.4) 20.7 (6.6)	15.4 (3.9) 20.7 (8.9) 16.7 (5.4)
Action potential properties			
Rheobase (pA)	323.5 (57.1) 218.2 (28.9)*** 216.9 (55.6)*** (K-W <i>P</i> = 0.0002) (K-W <i>P</i> < 0.0001)	420.0 (109) 447.6 (111.2) 428.6 (147)	446.3 (175.0) 361.4 (131.6) 371.2 (158.2)
Threshold (mV)	−37.9 (3.0) −43.2 (2.6)*** −41.4 (2.5)* (One-way ANOVA <i>P</i> < 0.0001) (One-way ANOVA <i>P</i> = 0.039) (One-way ANOVA <i>P</i> = 0.038)	−38.1 (5.8) −42.9 (4.8)* −39.4 (5.6) (K-W <i>P</i> = 0.023)	−46.4 (4.7) −47.8 (3.9) −46.9 (3.6)
Amplitude (mV)	71.4 (5.7) 76.1 (4.4) 72.1 (7.1)	84.5 (9.2) 90.5 (6.9) 86.8 (9.2)	94.1 (6.2) 95.4 (8.7) 91.2 (9.4)
Overshoot (mV)	35.3 (5.4) 34.9 (4.7) 33.5 (5.6)	46.2 (5.4) 47.8 (4.8) 47.2 (6.2)	49.5 (5.0) 49.8 (7.3) 46.3 (7.5)
Half-width (ms)	1.1(0.3) 1.3 (0.4) 0.9 (0.11) (One-way ANOVA <i>P</i> = 0.0048)	0.72 (0.15) 0.82 (0.12) 0.83 (0.2)	0.78 (0.15) 0.91 (0.30) 0.78 (0.15)

Values are presented as the mean (SD). Statistics: one-way ANOVA with Tukey's correction for multiple comparisons or Kruskal–Wallis test with Dunn's correction for multiple comparisons (K-W). The *P*-values are indicated when there is a significant statistical difference. *KCNQ2*<sup>WT/WT</sup> in XE-991 vs. *KCNQ2*<sup>WT/WT</sup> (green); *KCNQ2*<sup>WT/WT274M</sup> vs. *KCNQ2*<sup>WT/WT</sup> (blue); *KCNQ2*<sup>WT/WT</sup> in XE-991 vs. *KCNQ2*<sup>WT/WT274M</sup> (black). \**p* < 0.05, \*\**p* < 0.01, \*\*\**p* < 0.001. *C<sub>m</sub>*, membrane capacitance; PND, postnatal day; *R<sub>m</sub>*, membrane input resistance; *τ<sub>m</sub>*, membrane time constant; *V<sub>m</sub>*, resting membrane potential

for layers II/III. We observed that pyramidal cells of layer V presented some differences in their sensitivity to XE-991 and to the variant compared with pyramidal cells of layers II/III. In particular, at PND 7–9, cells (*n* = 16 wild-type cells from three animals) were affected neither by the variant (*n* = 17 mutant cells from three animals) nor by the Kv7 channel blocker (*n* = 10 XE-991-treated

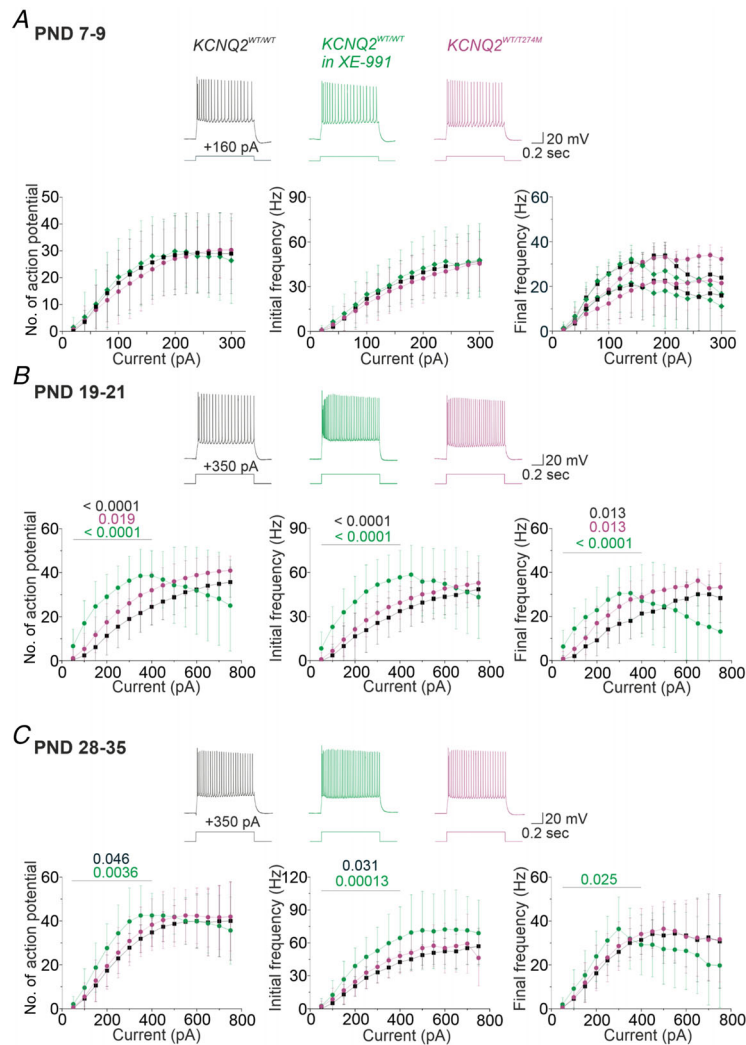
wild-type cells from three animals; Figs 3A and 4A and Table 2). At PND 19–21, the variant increased slightly but significantly the firing of pyramidal cells elicited by injection of current steps and affected only few parameters of the response elicited by the injection of a slow ramp of current (*n* = 18 wild-type cells from five animals and *n* = 20 mutant cells from five animals),



The Journal of Physiology

**Figure 2. Effects of XE-991 and of the p.T274M variant on the voltage responses of developing layers II/III pyramidal cells to the injection of a ramp of current**

A, traces showing the response of pyramidal cells to the injection of a ramp of 300 pA in 10 s recorded in motor cortical slices from *KCNQ2*<sup>WT/WT</sup> (black), *KCNQ2*<sup>WT/WT</sup> in the presence of XE-991 (green) and *KCNQ2*<sup>WT/T274M</sup> (blue) mice aged 1 week [postnatal day (PND) 7–9]. Below the traces are boxplots for quantification in the three groups of cells of the resistance, the current and voltage threshold of first action potential generation, the number of action potentials (APs), the initial frequency (first 200 ms of the discharge) and the variation of the membrane potential produced by a ramp of current of 300 pA. Black, wild-type cells (*n* = 16 cells from two animals); green, XE-991-treated wild-type cells (*n* = 11 cells from two animals); blue, mutant cells (*n* = 17 cells from three animals). B, same as in A in cells from mice aged 3 weeks (PND 19–21). Analyses were performed on the voltage responses to the injection of a ramp of current of 500 pA in 10 s. Black, wild-type cells (*n* = 20 cells from four animals); green, XE-991-treated wild-type cells (*n* = 21 cells from four animals); blue, mutant cells (*n* = 22 cells from four animals). C, same as in B in cells from mice aged 4–5 weeks (PND 28–35). Black, wild-type cells (*n* = 27 cells from five animals); green, XE-991-treated wild-type cells (*n* = 25 cells from five animals); blue, mutant cells (*n* = 25 cells from four animals). Statistical analysis was by one-way ANOVA with Tukey's correction for multiple comparisons or the Kruskal–Wallis test with Dunn's correction for multiple comparisons. The *P*-values are indicated when there is a significant statistical difference. The *P*-values are also given in the statistical summary table. Green, *KCNQ2*<sup>WT/WT</sup> (wild-type cells) vs. *KCNQ2*<sup>WT/WT</sup> in XE-991 (XE-991-treated wild-type cells); blue, *KCNQ2*<sup>WT/WT</sup> (wild-type cells) vs. *KCNQ2*<sup>WT/T274M</sup> (mutant cells); black, XE-991-treated wild-type cells vs. mutant cells.



The Journal of  
Physiology

**Figure 3. Effects of XE-991 and of the p.T274M variant on the discharge of developing pyramidal cells of layer V elicited by the injection of current steps**

A, representative traces showing the voltage responses to the injection of a current step of 160 pA for 1 s in layer V pyramidal cells in motor cortical slices from *KCNQ2*<sup>WT/WT</sup> (black), *KCNQ2*<sup>WT/WT</sup> in the presence of XE-991 (green) and *KCNQ2*<sup>WT/T274M</sup> (purple) mice aged 1 week [postnatal day (PND) 7–9]. Below the traces is shown the quantification (mean  $\pm$  SD) of the number of action potentials (left graph) elicited by the injection of depolarizing current steps, and the initial and final frequencies of the discharge (middle and right graphs, respectively) in pyramidal cells from animals aged 1 week. Black, wild-type cells ( $n = 16$  cells from three animals); green, XE-991-treated wild-type cells ( $n = 10$  cells from three animals); purple, mutant cells ( $n = 17$  cells from three animals). B, same as in A but for animals aged 3 weeks (PND 19–21). Traces depicted show voltage responses of pyramidal cells to the injection of a current step of 350 pA. Quantifications were done on 18 wild-type cells from five animals (black), 19 XE-991-treated wild-type cells from four animals (green) and 20 mutant cells from five animals (purple). C, same as in B but from animals aged 4–5 weeks (PND 28–35). Quantifications were done on 22 wild-type cells from five animals (black), 18 XE-991-treated wild-type cells from five animals (green) and 20 mutant cells from four animals (purple). Statistical comparisons (two-way repeated-measures ANOVA with Benjamini–Hochberg correction for multiple comparisons) were made on measurements from the starting point of the curve (for an injected current of 20 or 50 pA) to saturation of the response at each developmental stage. The *P*-values are indicated when there is a significant statistical difference. The *P*-values are also indicated in the statistical summary table. Green, XE-991-treated wild-type cells vs. wild-type cells; purple, mutant cells vs. wild-type cells; black, XE-991-treated wild-type cells vs. mutant cells. Underlying numerical values can be found in the statistical summary table (for A, number of action potentials, to C, final frequency).

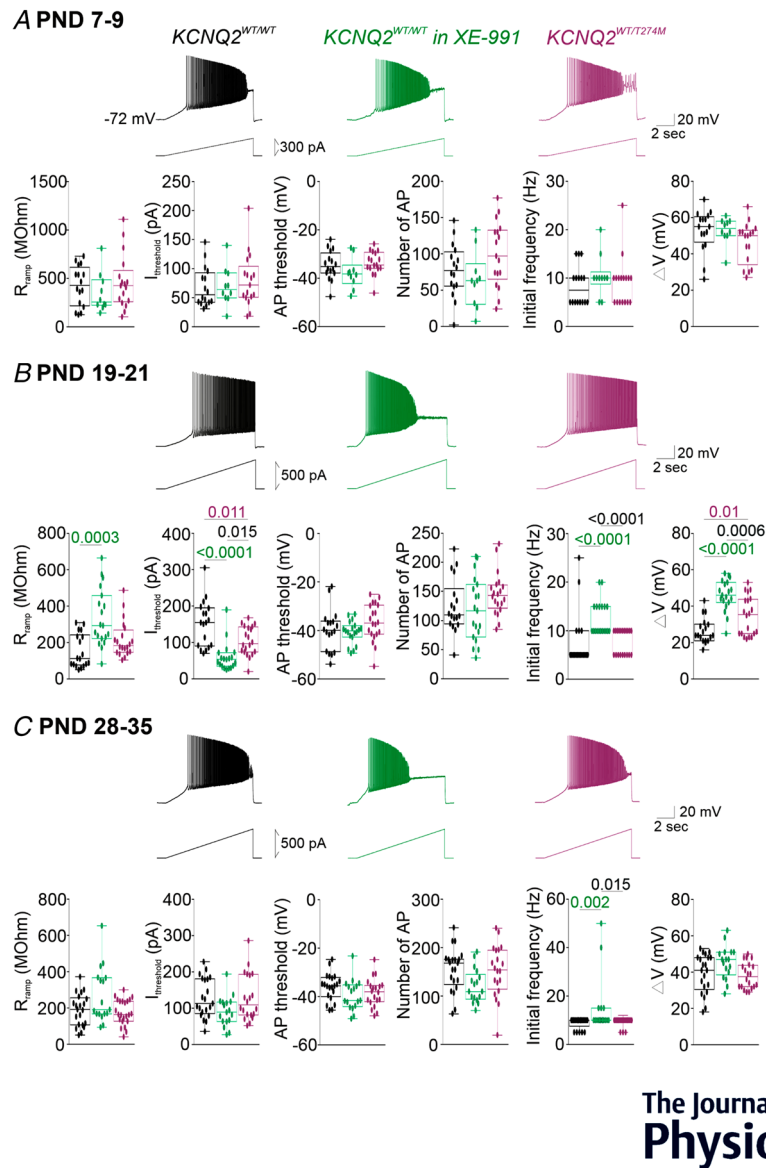


**Figure 4. Effects of XE-991 and of the p.T274M variant on the voltage responses of developing pyramidal cells of layer V to the injection of a ramp of current**

A, traces showing the response of pyramidal cells to the injection of a ramp of 300 pA in 10 s recorded in motor cortical slices from  $KCNQ2^{WT/WT}$  (black),  $KCNQ2^{WT/WT}$  in the presence of XE-991 (green) and  $KCNQ2^{WT/T274M}$  (purple) mice aged 1 week [postnatal day (PND) 7–9]. Below the traces, boxplots quantify, in the three group of cells, the resistance ( $R_{ramp}$ ), the current threshold ( $I_{threshold}$ ) and voltage threshold of first action potential (AP) generation, the number of action potentials, the initial frequency (first 1 s of the discharge) and the variation of the membrane potential ( $\Delta V$ ) produced by the ramp of current of 300 pA. Black, wild-type cells ( $n = 16$  cells from three animals); green, XE-991-treated wild-type cells ( $n = 10$  cells from three animals); purple, mutant cells ( $n = 17$  cells from three animals). B, same as in A in cells from mice aged 3 weeks (PND 19–21). Analyses were performed on the voltage response elicited by the injection of a ramp of 500 pA in 10 s. Black, wild-type cells ( $n = 18$  cells from five animals); green, XE-991-treated wild-type cells ( $n = 19$  cells from four animals); purple, mutant cells ( $n = 20$  cells from five animals). C, same as in B in cells from mice aged 4–5 weeks (PND 28–35). Black, wild-type cells ( $n = 22$  cells from five animals); green, XE-991-treated wild-type cells ( $n = 18$  cells from five animals); purple, mutant cells ( $n = 20$  cells from four animals). Statistical analysis was by one-way ANOVA with Tukey's correction for multiple comparisons or the Kruskal–Wallis test with Dunn's correction for multiple comparisons. The  $P$ -values are indicated when there is a significant statistical difference. The  $P$ -values are also indicated in the statistical summary table. Green, XE-991-treated wild-type cells vs. wild-type cells; purple, mutant cells vs. wild-type cells; black, XE-991-treated wild-type cells vs. mutant cells.

**Table 2.** Intrinsic properties of pyramidal cells of layer V in motor cortical slices from *KCNQ2*<sup>WT/WT</sup> mice (black), *KCNQ2*<sup>WT/WT</sup> mice superfused with XE-991 (20 μM, green) and *KCNQ2*<sup>WT/T274M</sup> mice (purple) aged 1, 3 and 4–5 weeks

Layer V	PND 7–9	PND 19–21	PND 28–35
	<i>KCNQ2</i> <sup>WT/WT</sup> <i>KCNQ2</i> <sup>WT/WT</sup> in XE-991 <i>KCNQ2</i> <sup>WT/T274M</sup>	<i>KCNQ2</i> <sup>WT/WT</sup> <i>KCNQ2</i> <sup>WT/WT</sup> in XE-991 <i>KCNQ2</i> <sup>WT/T274M</sup>	<i>KCNQ2</i> <sup>WT/WT</sup> <i>KCNQ2</i> <sup>WT/WT</sup> in XE-991 <i>KCNQ2</i> <sup>WT/T274M</sup>
<i>C<sub>m</sub></i> (pF)	54.9 (25.8) 57.0 (13.2)	109.9 (32.6) 99.9 (51.6)	111.8 (38.1) 101.1 (42.8)
<i>V<sub>m</sub></i> (mV)	51.8 (29.9) −63.1 (5.4) −63.3 (2.3) −61.2 (6.6)	119.6 (33.8) −69.4 (4.8) −68.1 (6.8) −71.1 (4.1)	114.1 (36.8) −68.9 (6.6) −68.9 (5.9) −69.2 (4.5)
<i>R<sub>m</sub></i> (mΩ)	515.6 (240.6) 451.0 (207.1) 482.3 (230.2)	126.6 (88.4) 262.7 (148.4) <sup>***</sup> 145.5 (65.8) (K-W <i>P</i> = 0.0008) (K-W <i>P</i> = 0.017)	158.5 (62.6) 208.9 (127.6) 160.6 (84.9)
<i>τ<sub>m</sub></i> (ms)	22.7 (8.4) 23.7 (7.0) 25.7 (9.7)	14.5 (10.1) 21.0 (9.2) 17.0 (6.7)	16.6 (7.5) 17.7 (10.8) 15.1 (5.7)
Action potential properties			
Rheobase (pA)	243.8 (90.4) 254 (66.7) 238.6 (72.5)	457.9 (137.7) 357.1 (113.2) 507.9 (135.6) (K-W <i>P</i> = 0.0008)	480.4 (133.8) 412.4 (129.3) 464.3 (168.9)
Threshold (mV)	−37.9 (4.0) −39.2 (6.8) −38.3 (6.0)	−47.9 (5.9) −46.3 (4.4) −45.6 (5.4)	−43.2 (5.5) −46.0 (5.1) −44.9 (4.0)
Amplitude (mV)	76.4 (9.5) 73.3 (7.2) 79.4 (5.7)	90.8 (5.7) 89.0 (8.0) 90.2 (7.0)	90.2 (6.5) 94.1 (6.5) 89.6 (6.6)
Overshoot (mV)	38.5 (5.1) 36.2 (8.9) 43.1 (8.1)	45.1 (4.8) 43.6 (6.4) 46.3 (8.8)	48.9 (6.7) 50.3 (5.1) 46.3 (4.8)
Half-width (ms)	1.3 (0.47) 1.5 (0.45) 1.1 (0.25)	0.70 (0.21) 0.83 (0.15) <sup>**</sup> 0.75 (0.15) (K-W <i>P</i> = 0.0023)	0.78 (0.2) 0.70 (0.09) 0.78 (0.17)

Values are presented as the mean (SD). Statistics: one-way ANOVA with Tukey's correction for multiple comparisons or Kruskal–Wallis test with Dunn's correction for multiple comparisons (K-W). The *P*-values are indicated when there is a significant statistical difference. *KCNQ2*<sup>WT/WT</sup> in XE-991 vs. *KCNQ2*<sup>WT/WT</sup> (green); *KCNQ2*<sup>WT/T274M</sup> vs. *KCNQ2*<sup>WT/WT</sup> (purple); *KCNQ2*<sup>WT/WT</sup> in XE-991 vs. *KCNQ2*<sup>WT/T274M</sup> (black). \**p* < 0.05, \*\**p* < 0.01, \*\*\**p* < 0.001. *C<sub>m</sub>*, membrane capacitance; PND, postnatal day; *R<sub>m</sub>*, membrane input resistance; *τ<sub>m</sub>*, membrane time constant; *V<sub>m</sub>*, resting membrane potential.

but the effects of the variant were of lower magnitude than those produced by XE-991 (*n* = 19 XE-991-treated wild-type cells from four animals; Figs 3B and 4B). At PND 28–35, as for pyramidal cells of layers II/III, the variant had no more consequences on layer V pyramidal cells, whereas XE-991 increased the neuronal discharge evoked by current steps and significantly increased the initial frequency of APs elicited by the injection of a ramp of current (*n* = 22 wild-type cells from five animals, *n* = 18 XE-991-treated wild-type cells from five animals and *n* = 21 mutant cells from four animals; Figs 3C and 4C).

Taken together, these data showed that the action of the p.T274M variant on neuronal excitability in layers II/III and V was developmentally regulated and that the relative contribution of Kv7/M channels to discharge of pyramidal cells in layers II/III and V is not equivalent.

#### Developmental effect of the p.T274M variant on M current in pyramidal cells of layers II/III and V

The increase in neuronal excitability produced by the variant is likely to be the consequence of a reduction in M current. Previous studies performed in heterologous

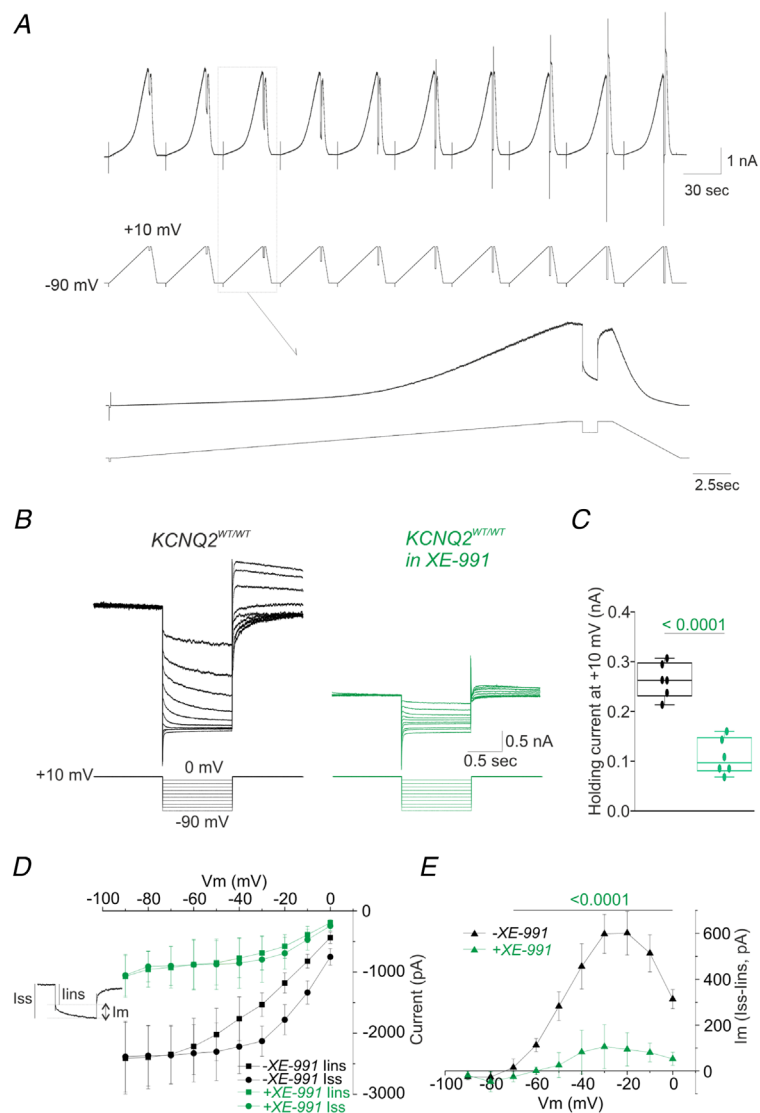
cells showed that the p.T274M variant reduced the M current carried by heteromeric Kv7.2/Kv7.3 channels by ~60% (Orhan et al., 2014) and by ~50% in interneurons of the locomotor CPG region of the spinal cord (Verneuil et al., 2020). We therefore analysed the impact of the variant on M current in pyramidal cells of layers II/III and V at the same three developmental stages from PND 7–9 to PND 28–35.

The M current was analysed using the standard  $I_m$  deactivation protocol described by Adams et al. (1982). Hyperpolarizing voltage steps down to -90 mV in 10 mV increments (1 s duration) were applied from a membrane potential of +10 mV (see Methods and Fig. 5A and B).

These hyperpolarizing steps led to a relaxation of inward current, the amplitude of which, calculated by subtracting  $I_{ss}$  from  $I_{ins}$  at each membrane potential, increased from 0 to -30 mV and then decreased at more hyperpolarized membrane potentials (Fig. 5D and E). The intersection of  $I_{ins}$  and  $I_{ss}$  yielded apparent reversal potentials ranging from ~-62 to -75 mV in wild-type cells of layers II/III and V depending on the developmental stage. Initially, in order to confirm that the current relaxation corresponded to the closing of Kv7 channels and the deactivation of M current, we recorded six wild-type pyramidal cells in layers II/III of motor cortical slices of the left hemisphere in the absence of XE-991 and six wild-type pyramidal

**Figure 5. Characterization of M current in pyramidal cells**

A, experimental protocol used to isolate M current. Slow ramps of voltage were applied from -90 mV to reach +10 mV in 30 s to activate Kv7/M channels. Cells were maintained for 1 s at this membrane potential, and hyperpolarizing voltage steps down to -90 mV (in 10 mV increments) were applied to deactivate the channels, leading to an inward current relaxation. The bottom traces show, at a higher time scale, an example of the current response to a slow ramp of voltage followed by a hyperpolarizing voltage step to -20 mV. B, isolated current responses to command hyperpolarizing voltage steps applied from +10 mV down to -90 mV recorded in a wild-type layers II/III pyramidal cell in a left motor cortical slice at postnatal day (PND) 20 in the absence of XE-991 and from another pyramidal cell in a right motor cortical slice from the same preparation in the presence of XE-991 (20  $\mu$ M). C, boxplot quantification of the mean holding current measured at +10 mV in cells recorded in the absence ( $n = 6$  cells, black) and in the presence of XE-991 ( $n = 6$  cells, green). D, left graph, instantaneous ( $I_{ins}$ , squares) and steady-state ( $I_{ss}$ , circles)  $I$ - $V$  relationships of wild-type cells in the absence (black symbols) and presence of XE-991 (green symbols). The apparent reversal potential of the current is the intersection between the two curves. E, graph showing the amplitude of the inward current relaxation measured as the difference between instantaneous and steady-state levels at the onset and end of each hyperpolarizing voltage step command. Current relaxation represents the deactivation of Kv7/M channels. Underlying numerical values can be found in the statistical summary table (for D and E). [Colour figure can be viewed at [wileyonlinelibrary.com](http://wileyonlinelibrary.com)]



cells in layers II/III of motor cortical slices of the right hemisphere from same animal aged 3 weeks and in presence of XE-991 (20  $\mu$ M). The presence of the Kv7 channel blocker led to a lower holding current at +10 mV and to a strong reduction (by  $\sim$ 85%) of the current relaxation at all membrane potentials (Fig. 5). These data demonstrated that the inward relaxation was mediated by  $I_m$ .

The M current was present in pyramidal cells of layers II/III at PND 7–9 and was sensitive to the p.T274M variant. We measured current density ( $I$ ) and calculated conductance ( $G$ ) at each membrane potential ( $I$ – $V$  and  $G$ – $V$  relationships, respectively). In comparison to wild-type cells, both  $I$ – $V$  and  $G$ – $V$  relationships of mutant cells were significantly smaller ( $n = 16$  wild-type cells from three animals and  $n = 16$  mutant cells from four animals; Fig. 6A). The apparent reversal potential (inter-section of  $I_{ss}$  and  $I_{ins}$ ) was, on average, not significantly affected by the variant ( $-66.3 \pm 2.2$  and  $-61.9 \pm 2.9$  mV in wild-type and mutant cells, respectively; Student's unpaired  $t$  test,  $P = 0.21$ ). At PND 19–21, current density and conductance measured in wild-type cells were  $\sim$ 4 and  $\sim$ 5 times higher, respectively, than at PND 7–9 ( $n = 17$  wild-type cells from four animals). The apparent reversal potential was also significantly more hyperpolarized ( $-75.6 \pm 1.3$  mV; Student's unpaired  $t$  test,  $P = 0.0007$ ). Both  $I$ – $V$  and  $G$ – $V$  relationships were significantly smaller in mutant cells compared with wild-type cells at PND 19–21, without any consequences for the reversal potential ( $-72.6 \pm 1.6$  mV; Student's unpaired  $t$  test,  $P = 0.16$ ;  $n = 16$  mutant cells from four animals; Fig. 6B). At PND 28–35,  $I$ – $V$  and  $G$ – $V$  relationships in wild-type cells were significantly smaller than in wild-type cells at PND 19–21 (two-way RM-ANOVA between 0 and  $-60$  mV,  $P = 7 \times 10^{-5}$  and  $P = 0.015$ , respectively;  $n = 16$  wild-type cells from three animals; Fig. 6B and C), whereas both relationships were similar in mutant cells at these two developmental stages (two-way RM-ANOVA,  $P = 0.46$  and  $P = 0.34$ , respectively;  $n = 16$  mutant cells from four animals at PND 28–35, Fig. 6B and C). Reversal potentials in wild and mutant cells were  $-74.3 \pm 1.5$  and  $-74.4 \pm 2.2$  mV, respectively. Importantly, at PND 28–35,  $I$ – $V$  and  $G$ – $V$  relationships in both groups of cells were not different (two-way RM-ANOVA,  $P = 0.42$  and  $P = 0.3$ , respectively; Fig. 6C). Finally, the p.T274M variant did not alter the deactivation time constant measured between 0 and  $-60$  mV at the three developmental stages. There were also no major variations of the time constant values measured at each membrane potential from PND 7–9 to PND 28–35.

In wild-type pyramidal cells of layer V, current density and conductance increased from PND 7–9 ( $n = 18$  wild-type cells from four animals) to PND 19–21 ( $n = 16$  wild-type cells from four animals) by  $\sim$ 4- and  $\sim$ 9-fold, respectively, with no further increase at PND 28–35 ( $n = 17$  wild-type cells from five animals; Fig. 7A–C).

However current density and conductance at PND 7–9 and PND 19–21 were significantly smaller than in layers II/III at the same two developmental stages (two-way RM-ANOVA at PND 7–9,  $P = 6 \times 10^{-6}$  and  $P = 5 \times 10^{-5}$  for  $I$ – $V$  and  $G$ – $V$ , respectively; at PND 19–21,  $P = 4 \times 10^{-7}$  and  $P = 0.0004$  for  $I$ – $V$  and  $G$ – $V$ , respectively). At PND 28–35,  $I$ – $V$  and  $G$ – $V$  relationships were similar in layer V and layers II/III (two-way RM-ANOVA,  $P = 0.12$  and  $P = 0.17$  for  $I$ – $V$  and  $G$ – $V$ , respectively). As shown in Figure 7, in layer V, the M current density and conductance were significantly reduced by the p.T274M variant only at PND 19–21 ( $n = 15$  mutant cells from three animals).

Taken together, these data showed that the p.T274 variant exerted a loss-of-function effect on Kv7/M channels in neocortical pyramidal cells and, as for the analysis of neuronal excitability, the effect was developmentally regulated and no longer observed in animals aged 4–5 weeks. Moreover, these data showed that the expression of M current was stronger in layers II/III than in layer V until the postweaning stage but reached a similar level at the juvenile stage.

### Spontaneous network-driven events are increased in motor cortical slices from $KCNQ2^{WT/T274M}$ mice

We next analysed spontaneous synaptic activity mediated by GABA and glutamate receptors at the same three developmental periods in layers II/III and V in motor cortical slices from  $KCNQ2^{WT/WT}$  and  $KCNQ2^{WT/T274M}$  mice. For this purpose, pyramidal cells located in these layers were recorded in the whole-cell configuration in voltage-clamp mode using patch pipettes filled with a caesium gluconate solution. Postsynaptic currents mediated by GABA<sub>A</sub> receptors (GABA<sub>A</sub>-PSCs) were recorded at 0 mV, the reversal potential of glutamate, whereas those mediated by glutamate receptors (GluR-PSCs) were recorded at the reversal potential of GABA, estimated to be  $\sim$ –70 mV in our recording conditions. Before adopting the whole-cell configuration, pyramidal cells were also recorded for 1–2 min in the tight cell-attached configuration (2–5 G $\Omega$ ) using same pipette solution.

In the cell-attached configuration, wild-type and mutant pyramidal cells of layers II/III and V recorded between PND 7 and 35 were either silent at their resting membrane potential or, when active, the firing of APs was very low ( $<10$  in 1 min; Fig. 8A). In the whole-cell configuration, spontaneous postsynaptic events recorded in both populations of cells and in the three developmental periods were mediated mainly by GABA<sub>A</sub> receptors. The frequency of these events was 3–10 times higher than that of GluR-PSCs (Fig. 9). In addition, the activity recorded at 0 mV included recurrent outward currents

with a magnitude of a few hundreds of picoamperes lasting between 0.5 and 2 s (Figs 8A and B and 9A and D). These large events were network activities resulting from the periodic summation of GABAergic postsynaptic currents. Indeed: (i) their frequency did not change with the membrane potential; (ii) they reversed polarity at

the reversal potential of GABA<sub>A</sub> receptors; (iii) they were insensitive to NBQX/APV ( $n = 4/4$  cells); and (iv) they were fully blocked by gabazine ( $n = 4/4$  cells; Fig. 8B).

These recurrent activities [recurrent GABAergic network activities (RGNA)] were recorded until

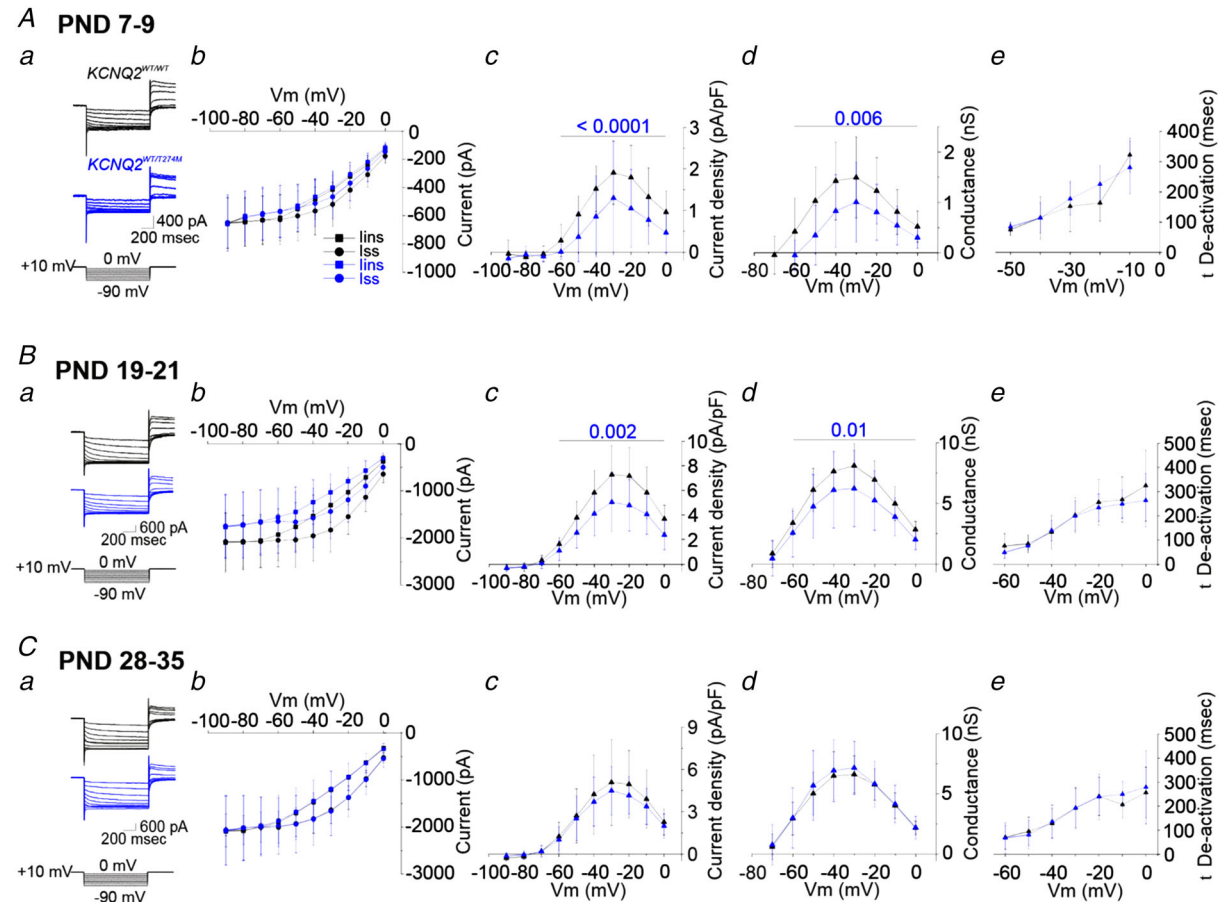


**Figure 6. Analysis of M current in layers II/III pyramidal cells from developing *KCNQ2*<sup>WT/WT</sup> and *KCNQ2*<sup>WT/T274M</sup> mice**

Aa, representative current responses to hyperpolarizing voltage steps in a wild-type pyramidal cell (black) and a mutant pyramidal cell (blue) recorded at postnatal day (PND) 8 and 9, respectively. Ab, plots (mean ± SD) of instantaneous ( $I_{ins}$ ) and steady-state current ( $I_{ss}$ )–voltage relationships measured in wild-type cells ( $n = 16$  cells from four animals, black symbols) and in mutant cells ( $n = 16$  cells from four animals, blue symbols). Ac–e, plots (mean ± SD) of M current density (c), conductance (d) and deactivation time constant (e) vs. membrane potentials of wild-type and mutant pyramidal cells from animals aged 1 week (PND 7–9). B, same as in A for wild-type and mutant pyramidal cells from animals aged 3 weeks (PND 19–21;  $n = 17$  wild-type cells from four animals and  $n = 16$  mutant cells from four animals). C, same measurements performed at PND 28–35 in 16 wild-type cells (three animals) and 16 mutant cells (four animals). Traces in Ca are from wild-type and mutant cells recorded at PND 29 and 30, respectively. Statistical analysis was by two-way repeated-measures ANOVA performed for values between 0 and –60 mV. The *P*-values are indicated when there is a significant statistical difference. The *P*-values are also indicated in the statistical summary table. Underlying numerical values can be found in the statistical summary table (for Ab–Ce).

The Journal of  
**Physiology**

PND 19–21. They were absent in cells from mice aged 4–5 weeks.

We wondered whether RGNA were sensitive to XE-991. The RGNA frequency and the area of the outward current underlying RGNA were quantified in pyramidal cells of the layers II/III and V in the absence and presence of the blocker in slices from the wild-type mice aged 3 weeks. The RGNA were more frequent and their area larger in

pyramidal cells of layers II/III and V in the presence of XE-991 (20  $\mu$ M) than in the absence of the blocker, whereas the frequency of spontaneous GABAR-PSCs (events in and outside RGNA) was not affected (Fig. 8C). Moreover, in layer V, after the blockade of Kv7 channels, RGNA were observed in 89% of pyramidal cells (eight of nine cells from two animals), whereas in the absence of XE-991, RGNA were observed in only 43% of pyramidal

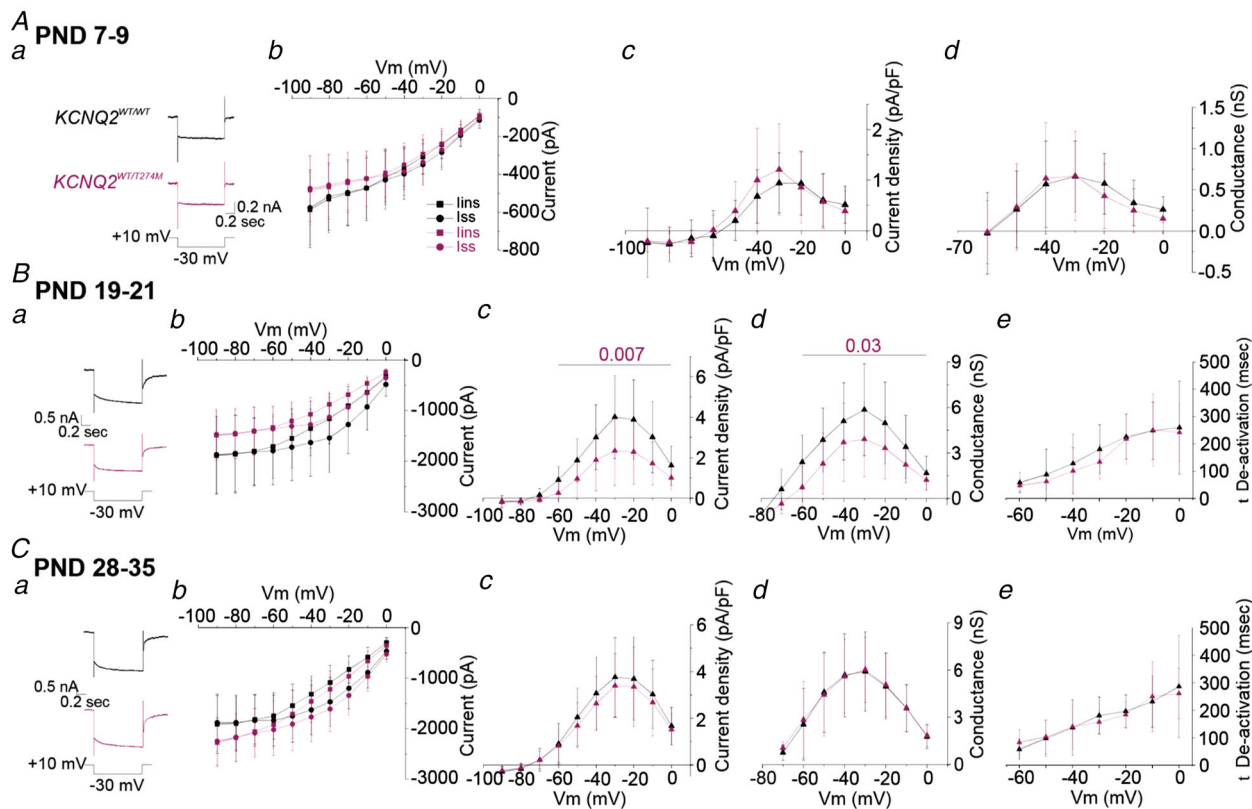


**Figure 7. Analysis of M current in pyramidal cells of layer V from developing  $KCNQ2^{WT/WT}$  and  $KCNQ2^{WT/T274M}$  mice**

Aa, representative current traces to a hyperpolarizing voltage step to  $-30$  mV in a wild-type pyramidal cell (black) and a mutant pyramidal cell (purple) recorded at postnatal day (PND) 7 and 9, respectively. Ab, plots (mean  $\pm$  SD) of instantaneous ( $I_{ins}$ ) and steady-state current ( $I_{ss}$ )–voltage relationships measured in wild-type cells ( $n = 18$  cells from four animals, black symbols) and in mutant cells ( $n = 16$  cells from four animals, purple symbols). Ac and Ad, plots (mean  $\pm$  SD) of M current density (c) and conductance (d) vs. membrane potentials of wild-type and mutant pyramidal cells from animals aged 1 week (PND 7–9). Measurement of the deactivation time constant was not done because of the very small amplitude of the currents in both wild-type and mutant pyramidal cells at this developmental stage. B, same as in A for wild-type and mutant pyramidal cells from animals aged 3 weeks (PND 19–21;  $n = 16$  wild-type cells from four animals and  $n = 15$  mutant cells from three animals). Traces in Ba are from wild-type and mutant cells recorded at PND 20 and 21, respectively. Be, plot of deactivation time constant vs. membrane potentials for wild-type and mutant cells. C, same measurements performed at PND 28–35 in 17 wild-type cells (five animals) and 17 mutant cells (four animals). Traces in Ca are from a wild-type cell and a mutant cell recorded at PND 29 and 30, respectively. Statistical analysis was by two-way repeated-measures ANOVA between 0 and  $-60$  mV. The  $P$ -values are indicated when there is a significant statistical difference. The  $P$ -values are also indicated in the statistical summary table. Underlying numerical values can be found in the statistical summary table (Ab–Ce).

The Journal of  
Physiology

cells (six of 14 cells from two animals). In layers II/III, RGNA were recorded in 100% of pyramidal cells (12 of 12 cells from two animals) in the absence of the blocker.

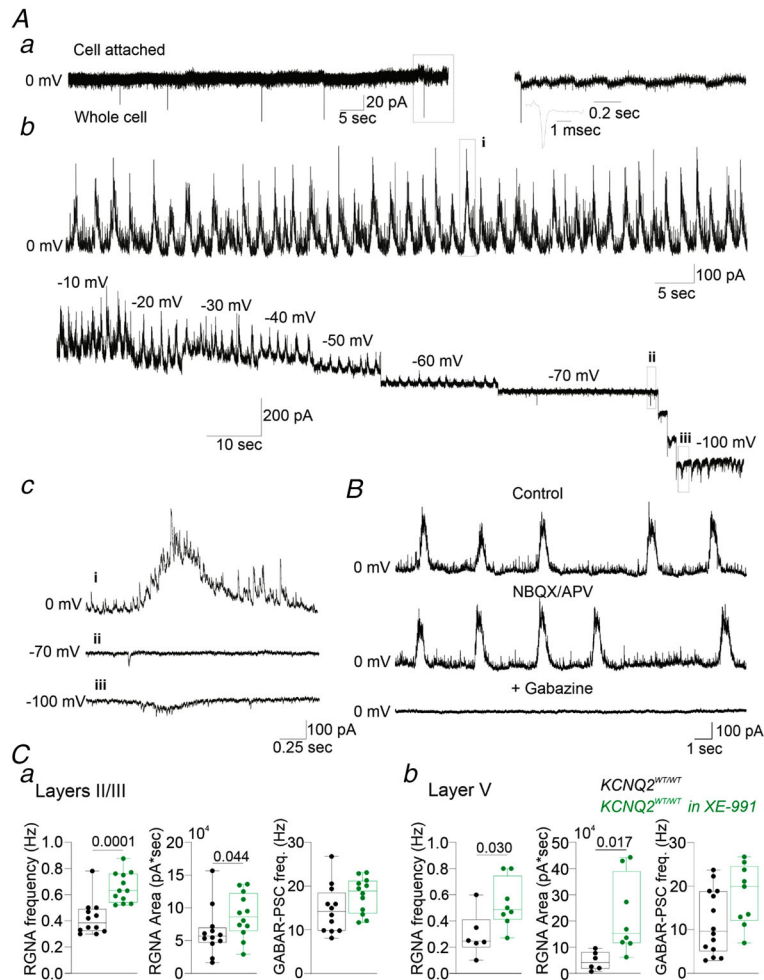
The RGNA were more often observed in wild-type pyramidal cells of layers II/III than of layer V. At PND 7–9, RGNA were recorded in 17 of 17 cells of layers II/III (three animals), occurring at frequencies ranging between 0.05 and 0.33 Hz (mean ± SD: 0.18 ± 0.09 Hz) and in 11 of 14 of cells of layer V (four animals) at frequencies ranging between 0.03 and 0.33 Hz (mean ± SD: 0.14 ± 0.10 Hz; Fig. 9A and D). At PND 19–21, RGNA were recorded in 27 of 31 cells of layers II/III (five animals, including the 12 wild-type cells and the two animals used in the above experiments) and at a frequency ranging between 0.1 and 0.8 Hz (mean ± SD: 0.36 ± 0.14 Hz) but in only 10 of 28 cells of layer V (five animals, including the 14 wild-type cells and the two animals used in the above experiments) at frequencies between 0.02 and 0.6 Hz,

which was, on average, significantly lower than in layers II/III (mean ± SD: 0.21 ± 0.18; Student's unpaired *t* test, *P* = 0.0117; Figs 8C and 9B and E). The RGNA were not observed in upper and deep layers in animals aged 4–5 weeks (layers II/III, *n* = 28 cells from four animals; layer V, *n* = 22 cells from three animals; Fig. 9C and F).

Having shown the sensitivity of RGNA to XE-991, we performed another series of experiments to determine whether RGNA were also affected by the variant. We observed that the p.T274M variant had consequences for RGNA in layers II/III. In these layers, at PND 7–9, the frequency of RGNA and the area of outward currents underlying RGNA in mutant pyramidal cells were increased significantly in comparison to RGNA recorded in wild-type pyramidal cells (*n* = 18 mutant cells from four animals; Fig. 9A). A small but significant increase in RGNA frequency but not in the area was also observed in mutant pyramidal cells at PND 19–21

**Figure 8. Recurrent GABAergic network activity in developing motor cortical slices**

**Aa**, pyramidal cell of layers II/III from a *KCNQ2*<sup>WT/WT</sup> mouse aged 3 weeks and recorded in the cell-attached configuration with a low action potential firing activity. Left trace shows one of these events (in the box) at a higher time scale. **Ab**, same cell recorded in the whole-cell configuration. Continuous recording of spontaneous activity was performed initially at 0 mV, then after the hyperpolarization of the membrane from 0 to –100 mV. The spontaneous activity is characterized by the presence of recurrent large outward currents reversing polarity at –70 mV, the frequency of which is insensitive to the membrane potential. Representative activities recorded at 0 (i), –70 (ii) and –100 mV (iii) are shown below in **Ac**. **B**, recurrent GABAergic network activity (RGNA) recorded in control conditions, in the presence of 2,3-dioxo-6-nitro-1,2,3,4-tetrahydrobenzo[*f*]quinoxaline-7-sulfonamide (NBQX; 10 μM) and D-2-amino-5-phosphonovalerate (D-APV; 40 μM) and after the addition of gabazine (5 μM). **C**, boxplots quantifying the frequency of RGNA, the area of the outward currents underlying RGNA, the total frequency of spontaneous GABA-mediated postsynaptic currents (events in and outside RGNA) in slices not treated (black) or treated with XE-991 (20 μM; green) and recorded in pyramidal cells of layer II/III (**Ca**) and V (**Cb**) from wild-type postweaning mice. Statistical analysis was by Student's unpaired *t* test and the Mann–Whitney *U* test. The *P*-values are indicated when there is a significant statistical difference. The *P*-values are also indicated in the statistical summary table. [Colour figure can be viewed at [wileyonlinelibrary.com](http://wileyonlinelibrary.com)]



( $n = 19$  cells from four animals; Fig. 9B). In addition, RGNA were recorded in 100% of the mutant cells but in 79% of wild-type cells (15 of 19 cells from three animals) in these new experiments. However, the frequency of

GABAR-PSCs (events in and outside RGNA) was not significantly different, suggesting that as with XE-991, most of the GABAR-PSCs were concentrated in the RGNA in the KI mice. The frequency of GABAR-PSCs

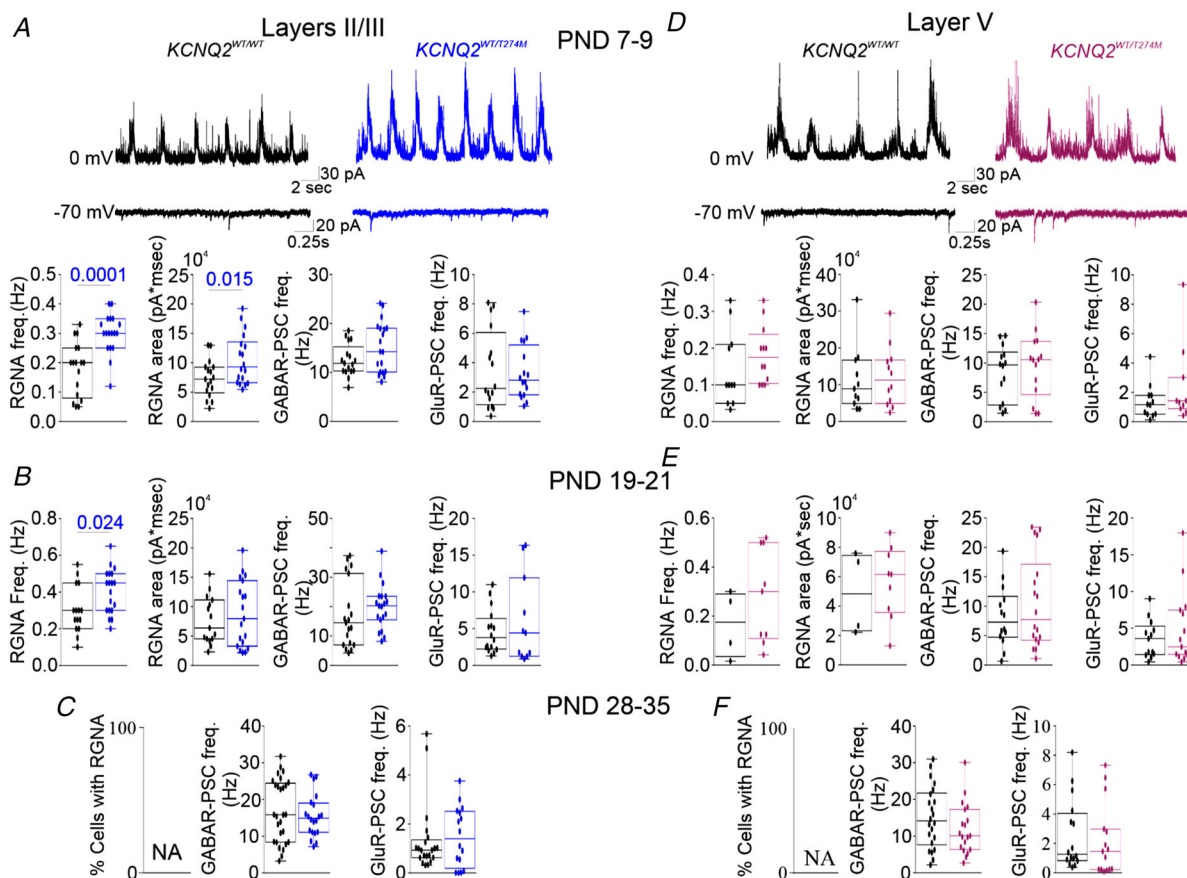


**Figure 9.** Effect of the p.T274M variant on spontaneous activities recorded in developing pyramidal cells of layers II/III and V

**A** and **D**, representative traces at postnatal day (PND) 7–9, showing spontaneous activities recorded at 0 and –70 mV in wild-type and mutant pyramidal cells of layer II/III (**A**, black and blue traces, respectively) and layer V (**D**, black and purple traces, respectively). Postsynaptic currents mediated by GABA<sub>A</sub> receptors (GABAR-PSCs) were recorded at 0 mV, whereas postsynaptic currents mediated glutamate receptors (GluR-PSCs) were recorded at –70 mV. Below the traces are boxplots quantifying the frequency of recurrent GABAergic network activity (RGNA), the area of the outward current underlying RGNA, the total frequency of spontaneous GABAR-mediated postsynaptic currents (events in and outside RGNA) and the frequency of GluR-PSCs recorded in pyramidal cells at PND 7–9. **B** and **E**, same quantifications in layer II/III and V pyramidal cells from mice aged 3 weeks (PND 19–21). **C** and **F**, same quantifications in cells from mice aged 4–5 weeks (PND 28–35). Recurrent GABAergic network activity was not observed (NA, not available). Statistical analysis was by Student's unpaired *t* test and the Mann–Whitney *U* test. The *P*-values are indicated when there is a significant statistical difference. The *P*-values are also indicated in the statistical summary table.

was also unaffected at PND 28–35 ( $n = 20$  mutant cells from four animals; Fig. 9C). There was also no significant difference in the frequency of GluR-PSCs between PND 7 and 35 (Fig. 9).

Ongoing synaptic activity recorded in layer V showed some differences from that recorded in layers II/III. As mentioned above, the occurrence of RGNA in wild-type cells of layer V and the number of cells in which they have been recorded were less than in layers II/III. At PND 19–21 in layer V, for these new experiments, RGNA were recorded in only 30% of cells (4 of 14 cells from three animals), and they occurred at lower frequencies than in layers II/III (mean  $\pm$  SD:  $0.3 \pm 0.13$  Hz,  $n = 15$  layer II/III pyramidal cells and  $0.16 \pm 0.17$  Hz,  $n = 4$  layer V pyramidal cells; Fig. 9E). The RGNA in layer V also appeared to be less sensitive to the variant. Thus, at both PND 7–9 and PND 19–21, there was no significant difference in the frequency of RGNA between wild-type cells ( $n = 14$  wild-type cells from three animals and 14 wild-type cells from three animals, respectively) and mutant cells ( $n = 14$  mutant cells from three animals and  $n = 18$  mutant cells from four animals, respectively; Fig. 9D and E). However, at PND 19–21, RGNA were recorded in 55% of mutant cells (10 of 18 cells) and in 28% of wild-type cells (4 of 14 cells). Therefore, as with XE-991, RGNA were observed more often in mutant than in wild-type pyramidal cells of layer V.

Finally, as for pyramidal cells of layers II/III, there were no significant differences in GABAR-PSC and GluR-PSC frequencies in wild-type cells and mutant cells of layer V in the three developmental periods studied ( $n = 22$  wild-type cells from four animals and  $n = 19$  mutant cells from four animals at PND 28–35; Fig. 9F).

Taken together, these data showed that RGNA recorded in layers II/III and V were sensitive to XE-991 and that the variant affected spontaneous synaptic activity only at developmental stages when RGNA were present and particularly in layers II/III. This suggested that GABAergic interneurons contributing to RGA in these layers might express M current carried by Kv7 channels, probably containing Kv7.2 subunit, although with a more limited effect of the variant in layer V.

### The contents of Kv7.2 and Kv7.3 in the developing motor cortex are not different in *KCNQ2*<sup>WT/WT</sup> and *KCNQ2*<sup>WT/T274M</sup> mice

We wondered whether the electrophysiological consequences of the variant and its time-dependent effect could be associated with a change in the expression levels of Kv7.2 and Kv7.3 subunits. Both subunits compose Kv7 channels in homomeric and heteromeric configurations and mediate M current in many cortical cells (Battfeld et al., 2014; Soh et al., 2014). We performed a western

blot of Kv7.2 and Kv7.3 in superficial and deep layers of the motor cortex from wild-type and KI mice aged 7, 21 and 30 days (Fig. 10A and C). We performed a classical two-way ANOVA to assess the effect of the variant on Kv7.2 and Kv7.3 subunits across age. The two factors considered were genotype and age. We did not observe a significant effect of the variant on Kv7.2 or Kv7.3 protein contents in either superficial or deep layers of the motor cortex at any age (Fig. 10B and D; see statistical summary table). Therefore, the age-dependent effect of the variant on electrophysiological activity was not associated with a change in the global production/expression of Kv7.2 and Kv7.3 subunits in the developing motor cortex.

### *KCNQ2*<sup>WT/T274M</sup> mice display spontaneous epileptic seizures preferentially at postweaning rather than at the juvenile stage

In a previous study (Milh et al., 2020), EEG monitoring after surgical implantation of electrocorticographic electrodes demonstrated the presence of seizures in  $\sim 20\%$  of *KCNQ2*<sup>WT/T274M</sup> mice (mean age PND 33). Based on our current electrophysiological results and given that seizures in patients disappear with age (Boets et al., 2021), we asked whether the occurrence of seizures would be regulated developmentally and higher in postweaning than in juvenile mice. For this purpose, intracranial EEG and video recording was performed in 32 *KCNQ2*<sup>WT/WT</sup> mice (16 at PND 18–21 and 16 at PND 35–50) and 32 *KCNQ2*<sup>WT/T274M</sup> mice (16 at PND 18–21 and 16 at PND 35–50) for a maximum of 48 h (see the Methods).

None of the 32 recorded *KCNQ2*<sup>WT/WT</sup> mice (from PND 18 to 50) showed abnormal behavioural or electrographic activity (Fig. 11A). In contrast, spontaneous seizures were detected in 60% of *KCNQ2*<sup>WT/T274M</sup> postweaning mice (10 of 16 KI mice), all occurring during sleep. Eight mice presented generalized seizures (Fig. 11Ba) with behavioural manifestations. These seizures were often violent, characterized by a two-stage pattern: an initial  $\sim 5$  s active running phase, during which the mice jumped and ran, followed by a 10–20 s tonic phase, during which the animals would fall and adopt a tonic posture with limb extension (see Supplemental Video 1). The active running phase was accompanied by a 3–5 s depolarization shift that saturated the amplifiers. During the tonic phase, a 3–5 Hz spike-and-wave discharge pattern appeared, progressively increasing in amplitude and frequency. At the end of the tonic phase, spike-and-wave discharge decreased in frequency, giving way to a flattening of the EEG and to the death of six mice. Two mice survived these seizures, with the EEG activity progressively resuming after 10–20 s of flattening.

Partial seizures were observed in two mice. In one mouse, the seizure consisted of a 3 Hz spike-and-wave

activity that was restricted to the right hemisphere (Fig. 11*Bb*). In the other, 5 Hz spike-and-wave activity was observed in only the right hippocampus (Fig. 11*Bc*; Supplemental Video 2). In both cases, there was no detectable behavioural activity.

As described in a previous study (Milh et al. 2020), spikes are observed in wild-type and KI animals. Spike frequency was quantified in 10 *KCNQ2*<sup>WT/T2474M</sup> mice (six that survived after seizures plus four that did not have seizures during the 48 h of recordings) and 14 *KCNQ2*<sup>WT/WT</sup> mice. Neocortical spikes were detected in eight *KCNQ2*<sup>WT/T2474M</sup> mice (mean rate of  $2.98 \pm 1.3$  spikes/h; range 0.1–11.7 spikes/h) and hippocampal spikes (mean rate of  $3.0 \pm 0.9$  spikes/h; range 0.04–8.13 spikes/h) in nine animals. Spikes tended

to occur in clusters (10–30 spikes/h during 30 min to 3 h), separated by prolonged periods (hours) of quiescence. They were generally detected simultaneously but at different amplitudes on all electrodes (Fig. 11*Ca*), but some focal spikes could also occur sporadically (Fig. 11*Cb*). In wild-type mice, rare spikes were detected in six of 16 mice, with six animals having neocortical spikes (mean rate of  $1.1 \pm 0.5$  spikes/h; range 0.03–3.1 spikes/h) and three mice having hippocampal spikes (mean rate of  $2.8 \pm 2.5$  spikes/h; range 0.08–7.9 spikes/h).

At PND 35–50, spontaneous epileptic seizures were recorded in only 25% of the *KCNQ2*<sup>WT/T2474M</sup> mice (4 of 16 KI mice). As in the postweaning mice, all seizures were violent, leading to the death of all four animals. The spike frequency was also quantified in 12 wild-type and

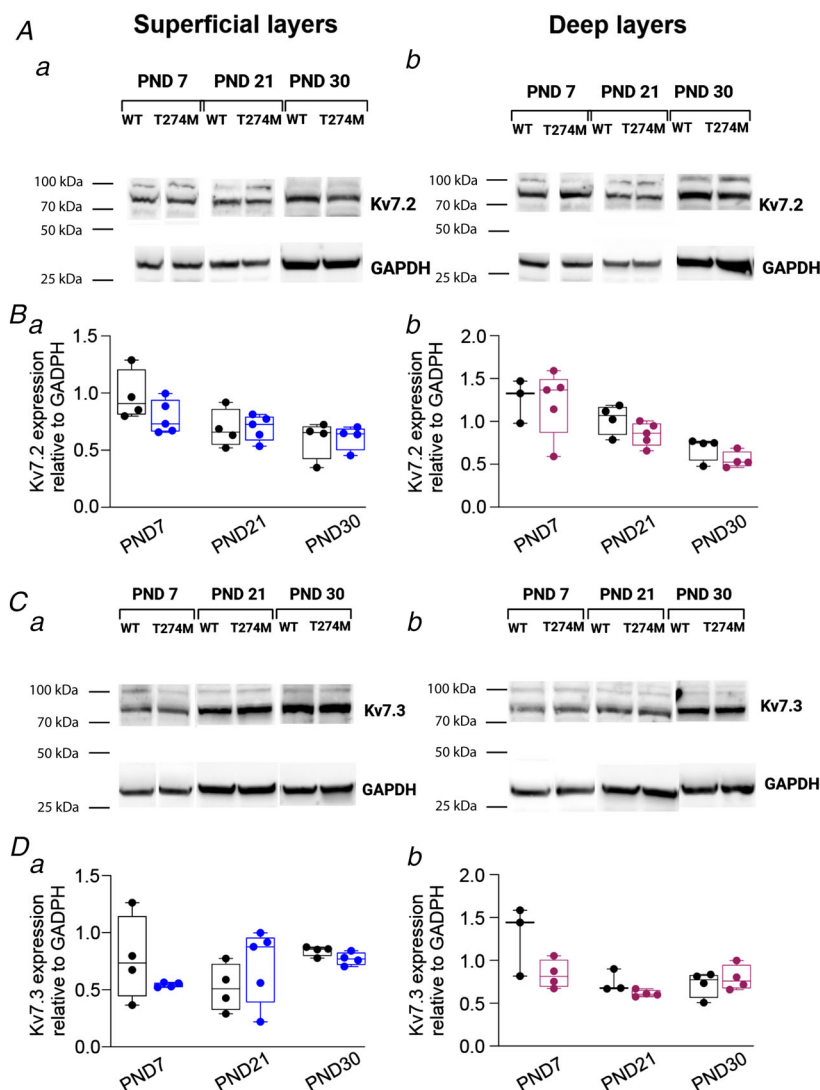


**Figure 10.** Kv7.2 and Kv7.3 subunits expression in superficial and deep layers in the motor cortex of developing *KCNQ2*<sup>WT/WT</sup> and *KCNQ2*<sup>WT/T274M</sup> mice

A, western blots of Kv7.2 and glyceraldehyde 3-phosphate dehydrogenase (GAPDH) at postnatal day (PND) 7, 21 and 30 in superficial layers (Aa) and deep layers (Ab). B, boxplots quantifying the Kv7.2 subunit relative to the housekeeping protein GAPDH in superficial (Ba) and deep layers (Bb) of the motor cortex from *KCNQ2*<sup>WT/WT</sup> (black dots) and *KCNQ2*<sup>WT/T274M</sup> mice (blue dots and purple dots) aged 7, 21 and 30 days. Each dot corresponds to quantification in one mouse. C, western blots of Kv7.3 and of GAPDH in both superficial (Ca) and deep layers (Cb). D, boxplots quantifying the Kv7.3 subunit relative to GAPDH in superficial (Da) and deep layers (Db) of the motor cortex from *KCNQ2*<sup>WT/WT</sup> (black dots) and *KCNQ2*<sup>WT/T274M</sup> mice (blue dots and purple dots) aged 7, 21 and 30 days. Statistical analysis for the effect of the variant across age was by two-way ANOVA. The two factors were the genotype and the age. For Ba, interaction  $P = 0.32$ , genotype  $P = 0.38$  and age  $P = 0.005$ . For Bb, interaction  $P = 0.83$ , genotype  $P = 0.21$  and age  $P = 0.0001$ . For Da, interaction  $P = 0.17$ , genotype  $P = 0.7$  and age  $P = 0.23$ . For Db, interaction  $P = 0.06$ , genotype  $P = 0.06$  and age  $P = 0.005$ . Statistical analysis for the comparisons of wild-type with knock-in (KI) mice at PND 7, 21 or 30 was by Student's unpaired  $t$  test and the Mann–Whitney  $U$  test. The  $P$ -values are given in the statistical summary table. [Colour figure can be viewed at [wileyonlinelibrary.com](http://wileyonlinelibrary.com)]

seven KI mice. In the neocortex, they were observed in two wild-type mice (0.11/h and 2.63/h) and in three KI mice at a rate of  $4.5 \pm 1.3/h$  (range 2.5–7/h). In the hippocampus they were detected in three wild-type mice at a rate of  $0.04 \pm 0.015/h$  (range 0.01–0.06/h) and in two KI mice (0.09/h and 0.11/h).

Taken together, these data confirmed that the p.T274M variant led to epileptic seizures in mice and indicated that brain excitability of postweaning KI mice was higher and more prone to generate epileptic seizures than that of juvenile mice.

## Discussion

In this study, we performed electrophysiological recordings in a mouse model of *KCNQ2*-related DEE carrying the loss-of-function p.T274M variant. This variant was identified in several patients (Milh et al., 2013, 2015; Orhan et al., 2014; Weckhuysen et al., 2012), therefore offering the opportunity to gain a better understanding of how dysfunction of Kv7 channel affects brain activity during development. Here, we provide evidence that the p.T274M variant leads to epileptic seizures *in vivo*

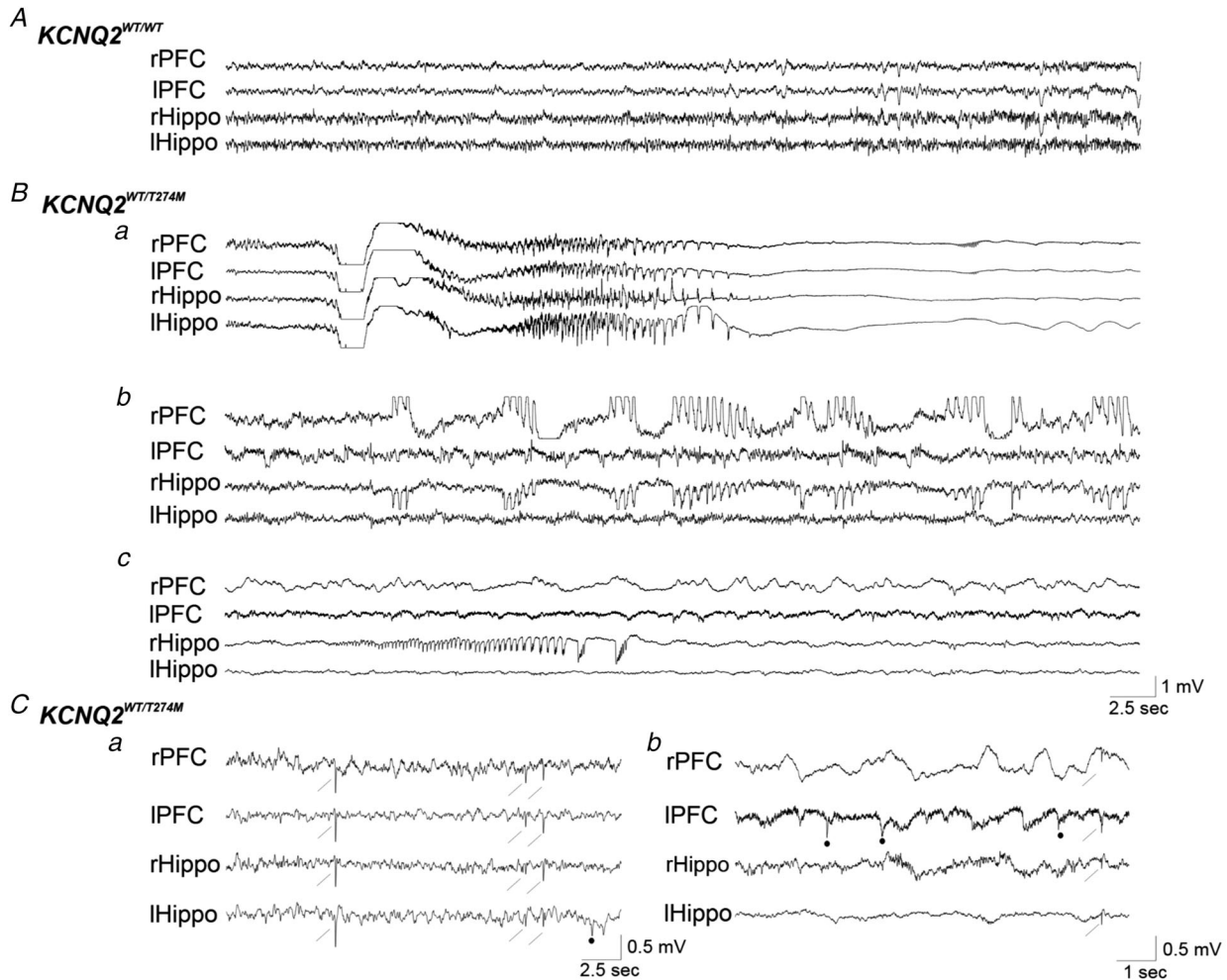


**Figure 11. Intracranial EEG recordings of postweaning mice**

Electrodes were implanted in the prefrontal cortex (PFC) and hippocampi (Hippo) of the right (r) and left (l) hemispheres. *A*, recordings from a *KCNQ2*<sup>WT/WT</sup> mouse. *B*, spontaneous seizures recorded in *KCNQ2*<sup>WT/T274M</sup> mice. *Ba*, generalized seizure, which represented the most frequent type of seizures encountered in mutant mice. *Bb* and *Bc*, partial seizures recorded in two mutant mice with epileptic activities observed in both prefrontal cortex and hippocampus of the right hemisphere (*Bb*) and with an epileptic discharge present only in the hippocampus of the right hemisphere (*Bc*). *C*, spikes recorded in two mutant mice. These spikes could be synchronized in the right and the left hemispheres (arrows) or be observed in only one structure of one hemisphere (black dot). [Colour figure can be viewed at [wileyonlinelibrary.com](http://wileyonlinelibrary.com)]

and, at cellular level, to a decrease of M current, an increase of pyramidal cell excitability and an increase of network-driven synaptic events, although with some differences depending on the cortical layers. Importantly, with respect to seizures, we show that these alterations are time limited, being observed until the postweaning stage and not later, at the juvenile stage, when the variant has no more consequences on Kv7/M channel function and on neuronal excitability.

Thus, we observed in layers II/III that there was a strong parallelism between the effect of the variant and of the M channel blocker XE-991 on the electrophysiological properties of pyramidal cells until PND 19–21. The responses of the cells to the injection of current were impacted in a similar manner by the variant or the blocker, with a general increase in neuronal excitability up to a certain level of current injected. These results are in keeping with the function of Kv7 channels in the control of neuronal excitability and, in particular, the fact that they play fundamental roles to limit neuronal firing and to reduce the frequency of the discharge. Moreover, the current ramp protocol, which should, in principle, reveal better the contribution of Kv7 channels to the neuronal response over inactivating ionic channels, showed that both mutant cells and XE-991-treated wild-type cells discharged at a higher frequency for a lower amount of current injected and generated a larger depolarization than in wild-type cells. These results also support the idea that the electrophysiological consequences of the variant on cellular properties are related to a decrease in M current and a concomitant increase in membrane resistance at potentials where the M current is normally activated. In keeping with this, we observed that M current density and conductance were reduced in mutant cells. We cannot exclude the possibility that other conductances are affected in mutant cells and participated in the neuronal hyperexcitability, as was shown recently for the calcium-activated BK and SK channels in human induced pluripotent stem cell-derived neurons expressing the *KCNQ2* p.R581Q pathogenic variant (Simkin et al., 2021).

Our data also indicated that Kv7 channels already control neuronal excitability in the motor cortex during the neonatal period. This was also described in acutely dissociated pyramidal cells and parvalbumin-like interneurons of layers II/III of the somatosensory cortex, CA1 and CA3 pyramidal cells of the hippocampus, and lumbar interneurons of the spinal cord from rodents aged 1 week (Guan et al., 2011; Marguet et al., 2015; Safiulina et al., 2008; Soh et al., 2018; Verneuil et al., 2020). Thus, Kv7/M channels already appear to be important modulators of firing properties of neurons from several regions at early developmental stage, and even if M current density is much lower at neonatal stage than at juvenile and adult stages, these channels are likely to play fundamental roles

for proper brain development and for preventing hyper-synchronicity of cellular activity (Hou et al., 2021; Marguet et al., 2015; Peters et al., 2005; Safiulina et al., 2008).

However, in the cell-attached configuration in wild-type cells and in both mutant cells and XE-991-treated wild-type cells of layers II/III and V, we did not observe the presence of spontaneous AP currents from neonatal to juvenile developmental stages. The absence of spontaneous activity is not surprising according to the resting membrane potential of cortical pyramidal cells measured in the whole-cell configuration ( $\sim -70$  mV), even in presence of XE-991, and according to the membrane threshold of APs. In addition, the resting membrane potential might be underestimated, particularly during the neonatal period, owing to the short-circuit effect of the leak through the contact between the electrode and the membrane in whole-cell recordings (Tyzio et al., 2003). Moreover, in a recent study aiming to analyse the electrophysiological consequences of the deletion of *KCNQ2* or *KCNQ3* at network level, Hou et al. (2021) performed calcium imaging, and rare calcium activity was detected in the neocortex from neonates in control (wild-type conditions) with a physiological extracellular concentration of  $K^+$  ( $[K^+]_o$ ; some modest activity was observed only in the hippocampus and in the entorhinal cortex). It was necessary to increase  $[K^+]_o$  from 2.5 to 8 mM to obtain calcium events in the neocortex and enhance the role of *KCNQ2* or *KCNQ3*. In another study, the consequences of deletion of *KCNQ2* or *KCNQ3* on neuronal firing in CA1 have also been analysed at PND 15–20 in the cell-attached configuration by the same group. An increase of  $[K^+]_o$  to 8.5 mM was necessary to obtain spontaneous firing of the cells (Soh et al., 2014). Finally, blockers or activators of Kv7 channels had effects on synaptic transmission in the CA1 region of the hippocampus only after increasing  $[K^+]_o$  to 10.5–11.5 mM (Vervaeke et al., 2006).

Therefore, cortical pyramidal cells might not discharge APs easily at their true resting membrane potential, at which the action of Kv7 channels is certainly very limited. To elicit a spike discharge and enhance the impact of Kv7 channels, it seems necessary to shift the reversal potential of potassium to depolarized values by increasing  $[K^+]_o$  (Soh et al., 2014).

Our results also suggest that the Kv7.2 subunit might contribute strongly to the M current in layers II/III. A recent study performed in the somatosensory cortex showed that the conditional ablation of *KCNQ2* or the transfection by electroporation of the pathogenic p.I205V variant related to DEE leads to a hyperexcitability of pyramidal cells of layers II/III, whereas conditional ablation of *KCNQ3* did not have such an impact (Niday et al., 2017; but see Hou et al., 2021). In the present study, we cannot exclude the contribution of other subunits to Kv7 channels in these cells, and in particular

Kv7.5, but if anything, this should be small regarding the large reduction of M current ( $\sim 85\%$ ) produced by the blocker at  $20 \mu\text{M}$ , while homomeric Kv7.5 or heteromeric Kv7.3/Kv7.5 subunits display low sensitivity to XE-991 (Schroeder et al., 2000).

The fact that in layers II/III both XE-991 and the p.T274M variant had equivalent consequences on the voltage response to current injection was, nevertheless, surprising regarding their respective effects on M current, with the variant reducing current density by  $\sim 30\text{--}40\%$ . There are at least two possible explanations: i) a more efficient blockade of Kv7 channels by XE-991 in voltage-clamp than in current-clamp experiments. Indeed, XE-991 operates better when channels are open (Greene et al., 2017), which is a situation that was favoured by the protocol used to study M current rather than to study neuronal excitability. However, this explanation is difficult to reconcile with the more powerful effects exerted by XE-991 over those produced by the variant in the response of layer V pyramidal cells at PND 19–21 to the injection of steps or a ramp of current; ii) a high sensitivity of pyramidal cells to Kv7 channel activity with a rapid saturation of the voltage response–current relationship. A similar sensitivity is certainly present in pyramidal cells of layer V at PND 19–21; alterations produced by the variant on both the voltage response and M current are within the same range as those produced in layers II/III. Moreover, the responses of wild-type cells to the injection of steps and a ramp of current were equivalent. The stronger effect produced by XE-991 certainly denotes a capacity for a voltage response to current injection that is larger in layer V than in layers II/III pyramidal cells.

An important difference between layers II/III and layer V pyramidal cells was the lack of effect of the variant and of XE-991 on the excitability of layer V pyramidal cells at PND 7–9. This is probably a consequence of the low level of M current in wild-type cells of layer V, which density was half that in layers II/III. It is possible that the M current in layer V is carried by channels that include the Kv7.5 subunit rather than Kv7.2; the Kv7.3/Kv7.5 association generating lower current than that carried by the Kv7.2/Kv7.3 association (Jentsch, 2000). By contrast, the Kv7.2/Kv7.3 association would conduct a large part of the current at PND 19–21 in layer V and from the neonatal period in layers II/III. It is well known that there are differences in the expression of ion channels and intrinsic properties of cells within the same structure. This has been documented, in particular, in the superficial and deep layers of CA1 and CA3 pyramidal cells, between the CA3 and CA1 pyramidal cells or between CA1 pyramidal cells of the dorsal and ventral hippocampus (Cembrowski & Spruston, 2019; Hönigspurger et al., 2015; Marissal et al., 2012; Mizuseki et al., 2011; Tzingounis et al., 2010).

Analysis of the M current showed an apparent reversal potential of  $\sim -74 \text{ mV}$  at the postweaning and juvenile developmental stages and even at a more depolarizing potential at PND 7–9, a mean value that deviates greatly from  $E_K$  calculated by Nernst equation ( $\sim -94 \text{ mV}$ ). A similar value of the M current reversal potential has been described in hypoglossal motoneurons from inward relaxation analysis (Ghezzi et al., 2017), whereas in the neocortical pyramidal cells or mossy fibre terminals the values were close to the calculated  $E_K$  (Battefeld et al., 2014; Martinello et al., 2019). This discrepancy is difficult to understand. The simplest explanation could be an imperfect clamp of the membrane when using a strong voltage command, particularly when the current is generated at a distance from the recording site, although the axon initial segment is close to the soma. In the studies performed by Battefeld et al. (2014) and Martinello et al. (2019), the M current was recorded at the axonal node (bleb) and at axon boutons, respectively, which are sites of concentrated Kv7 channels and that are of smaller size than the large soma of pyramidal cells where recording electrodes were positioned in the present study. There are also other possible explanations for the depolarized value of the reversal potential in our conditions. First, there might be contamination by another conductance responsible for an inward current. However, channels generating inward current were blocked in our experimental conditions. This is the case for voltage-gated  $\text{Na}^+$  and  $\text{Ca}^{2+}$  channels, in addition to HCN channels. Second, there might be a permeability of Kv7 channels to  $\text{Na}^+$ . Recent observations demonstrate in heterologous cells a physical interaction between Kv7.2 subunit and SMIT1, which enables the transport of myo-inositol into the cells and the raise of PIP2, a phosphoinositide that plays a crucial role in Kv7 channel function. The formation of this complex increases  $\text{Na}^+$  permeability, which, if present in cortical neurons, should deviate the reversal potential of M current from  $E_K$  (Manville et al., 2017). Third, as mentioned by Ghezzi et al. (2017), the Nernst equation does not take into account the presence of pumps, transporters and non-permeant anionic molecules in the cytoplasm, which might affect the spatial distribution and concentration of intracellular  $\text{K}^+$  (see also Rahmati et al., 2021). Further studies are necessary to clarify this point.

An important issue of the present study is that the action of the variant on the activity of neocortical pyramidal cells is time limited. Neither the membrane response to current injections nor M current density and conductance were significantly different in wild-type and mutant cells at PND 28–35. The similar level of excitability of mutant and wild-type cells is likely to be related to the lack of effect of the variant on Kv7 channels rather than to a lack of regulation of neuronal activity by these channels, because wild-type cells were still sensitive

to XE-991 at PND 28–35, although the blocker seems to have a lower impact on membrane responses to injection of currents at PND 28–35 than at PND 19–21. Our results show that M current in wild-type and mutant cells seems to have evolved differently in layers II/III and V at the postweaning and juvenile stages. In layers II/III,  $I-V$  and  $G-V$  relationships were significantly smaller in wild-type cells at PND 28–35 than at PND 19–21, whereas these relationships were stable in mutant cells, meaning that current density and conductance values in these cells approached those of wild-type cells at PND 28–35. This is the opposite in layer V, where at this developmental stage the  $I-V$  and  $G-V$  relationships were stable in wild-type cells but increased in mutant cells from PND 19–21 to PND 28–35. This indicates a different mode of regulation for the expression of M current in wild-type cells of layers II/III and V at these two developmental stages. In layers II/III, the down shift of both  $I-V$  and  $G-V$  relationships observed in wild-type cells at PND 28–35 did not occur in mutant cells, whereas in layer V it seems that it is rather an increase in Kv7 channel function in mutant cells that allows the similar  $I-V$  and  $G-V$  relationships with wild-type cells. These results suggest that at PND 28–35, different mechanisms are engaged in mutant cells of layers II/III and V to bring Kv7/M channel function to a physiological level and to abolish the effects of the variant on neuronal excitability. This could include post-translational mechanisms (phosphorylation/dephosphorylation or modulation by intracellular molecules) affecting Kv7 channel function. Our biochemical analysis did not reveal a significant effect of the variant on global expression of Kv7.2 and also Kv7.3 subunits in both superficial and deep layers across age. These data are in keeping with biochemical studies performed in *Xenopus* oocytes expressing the p.T274M variant (Orhan et al., 2014). However, our experiments do not allow us to exclude the possibility that subtle changes in subunit expression at the membrane and channel composition occurred at the single-cell level in juvenile KI mice.

Our data showed that the variant and XE-991 not only affected the properties of pyramidal cells but also probably affected the properties of interneurons. This was suggested from the analysis of spontaneous synaptic activity. We observed the presence of spontaneous network-driven events that were mediated by GABA receptors (called RGNA), and these were observed more often in layers II/III than in layer V. We found that RGNA were highly sensitive to XE-991 in both layers II/III and V and to the variant, particularly in layers II/III, where their frequency was increased in the KI mice. Spontaneous network-driven activities have been described in several developing structures, including the hippocampus (Ben-Ari et al., 1989, 2007; Garaschuk et al., 1998), the neocortex (Allene et al., 2008; Garaschuk

et al., 2000; Modol et al., 2017), where they were called giant depolarizing potential (GDPs) or early network oscillations (ENOs), the spinal cord (Landmesser & O'Donovan, 1984) and the retina (Meister et al., 1991). In the cortex, these patterns modify the efficacy of developing GABAergic and glutamatergic synapses and are likely to play an important role in the wiring of neuronal circuits, the alteration of which could be the cause of epilepsy and developmental delay (Ben-Ari et al., 2007; Griguoli & Cherubini, 2017; Khazipov & Milh, 2018). Interestingly, in the hippocampus, a change in the frequency of GDPs (increase or decrease) has been reported in some animal models of neurodevelopmental disorders (Griguoli & Cherubini, 2017). Moreover, GDPs, like RGNA, are also sensitive to Kv7/M channel blockers (Safiulina et al., 2008).

However, RGNA display some differences from GDPs/ENOs. First, they were still observed in the presence of glutamate receptor antagonists, suggesting that they do not necessitate pyramidal cell activation for their generation. Second, they seem to be mediated largely or exclusively by GABA receptors, whereas GDPs/ENOs contain a glutamatergic component (Khalilov et al., 2015). The fact that pyramidal cells were silent or fired rare APs (in the cell-attached configuration) during bursts of GABAR-PSCs probably explains why glutamate receptors did not contribute to RGNA. Third, RGNA are observed at PND 19–21, notably in layers II/III and with a higher frequency than at PND 7–9, whereas GDP/ENOs disappeared in cortical slices from rodents aged 1–2 weeks.

It is possible that the differences in the properties of RGNA and GDPs/ENOs are related to the cortical structure analysed and/or the rodents species used. In the hippocampus, synaptically driven network patterns are orchestrated by a subpopulation of pioneer early-born GABAergic interneurons expressing somatostatin, possessing widespread axonal arborization and acting as hub cells (Bonifazi et al., 2009; Picardo et al., 2011). The existence of GABAergic hub cells has also been described in the entorhinal cortex, and they are likely to exist in other neocortical regions, such as the motor cortex, to orchestrate network activity (Modol et al., 2017). We speculate that Kv7 channels incorporating Kv7.2 subunits play an important role in the firing properties of these cells. However, the reasons why the variant impacts RGNA in layers II/III but much less in layer V (RGNA were observed in a higher percentage of mutant cells at PND 19–21) while they were sensitive to XE-991 is difficult to understand, notably because some interneurons, including hub cells of both layers, might be interconnected, which would allow the propagation of RGNA from one layer to another (Jiang et al., 2015; Modol et al., 2017). At present, there are some data regarding the expression and function of Kv7 channels in interneurons. Studies have essentially been performed

in hippocampal interneurons, where expression and modulation of neuronal firing by Kv7 channels have been demonstrated for regular and fast spiking interneurons maintained in primary hippocampal cultures (Grigorov et al., 2014), in a subset of somatostatin oriens-lacunosum moleculare (OLM) interneurons and parvalbumin-expressing interneurons in the CA1 region of the hippocampus; in the basket cells, OLM and bistratified interneurons of the CA3 region (Fidzinski et al., 2015; Lawrence et al., 2006; Nieto-Gonzalez & Jensen, 2013; Soh et al., 2018). Other data provided also demonstrate the modulation of neuronal firing by Kv7 channels of parvalbumin-expressing interneurons in layers II/III of the somatosensory cortex (Soh et al., 2018). It is therefore not surprising that Kv7.2 variants affect spontaneous GABAergic activity in the neocortex (the present study) and the hippocampus (Uchida et al., 2017; but see Marguet et al., 2015). Although it is unclear whether RGNA have any correspondence *in vivo*, our data suggest that a population of interneurons, whose identity and properties remain to be characterized, are impacted by the variant and must play an important role in the pathophysiology of *KCNQ2*-related DEE.

Video and EEG monitoring revealed the presence of seizures, with or without behavioural manifestation. As described in previous studies (Milh et al., 2020), behavioural seizures, which account for most of the epileptiform events recorded, were associated with violent locomotor activity and usually terminated with the death of the animal. The synchronous spike-and-wave discharge pattern associated with such seizures is reminiscent of the patterns typically observed in generalized epilepsies. However, we also observed focal seizures, restricted to one hemisphere or one hippocampus. These seizure patterns were not associated with any behavioural manifestations. Despite the presence of seizures, we did not observe the suppression burst patterns that are typically observed in *KCNQ2*-related DEE patients in the neonatal period. However, given that our recordings were performed only after weaning, it is possible that we missed the temporal window when such patterns would occur in mice.

In view of the results obtained from the *ex vivo* recordings, how can we explain the fact that postweaning KI mice displayed spontaneous seizures? Although the GABAergic interneurons responsible for RGNA are expected to be more active spontaneously in KI mice than in wild mice, mutant pyramidal cells did not fire APs spontaneously; the hyperexcitability of these cells was unmasked after depolarizing current injections. However, *in vivo* these depolarizing currents could be provided by the different rhythmic activities/oscillatory patterns present in the brain, such as theta and gamma rhythms, spindles and sharp wave ripples. Owing to the lower rheobase of mutant cells, these patterns might facilitate their recruitment by crossing the AP threshold. Given

that mutant cells and probably some interneurons are equipped with altered Kv7 channel function, they fire more APs and at a higher frequency. Altogether, this might favour synaptic transmission and, more generally, increase the power of the connectivity between neurons, leading to cortical network recruitment and seizures. Thus, the changes produced by the variant in neuronal properties reduce the excitation threshold of affected cells, making KI mice more prone to seizures than wild-type mice. This notion of threshold has been documented in several animal models inactivated for specific genes related to epileptic disorders (such as *FlnA*, *EAAT*, *DCX* and *KCNQ2*<sup>+/-</sup> mice). These animals presented a higher seizure susceptibility to convulsive agents such as pentetrazole, temperature elevation or kainic acid (Carabolana et al., 2012; Kim et al., 2020; Petit et al., 2014; Tanaka et al., 1997; Watanabe et al., 2000).

During the revision of the present manuscript, an article was published describing the phenotype of a conditional transgenic mouse expressing the pathogenic variant p.M547V (corresponding to p.M546V variant-related DEE in humans) in forebrain pyramidal cells (Kim et al., 2021). The authors showed that these conditional KI mice displayed abnormal behaviour at PND 21 and, as we found, spontaneous lethal tonic-clonic seizures, but as early as PND 60–85. Therefore, the impact of a given pathogenic variant of *KCNQ2* might vary according to its location. Although electrophysiological recordings have not yet been performed in this model, the differential effect of the two variants during development shows how complex the pathophysiology of *KCNQ2*-related DEE might be (Allen et al., 2020; Dirckx et al., 2020; Milh et al., 2013).

In summary, we showed that the p.T274M variant clearly affected the properties of cortical cells and ongoing synaptic activity, which might contribute to epileptic seizures. Our data also showed that the electrophysiological consequences of Kv7 channel dysfunction *in vivo* and *ex vivo* was transient and observed during a restrained period of development. These findings are particularly relevant to *KCNQ2*-related DEE, given that for a majority of patients, a normalization of the electrographic activity and remission of the epilepsy few weeks to several months after the onset of seizures is often observed, whereas the neurological outcome remains poor. In particular, the epilepsy of one patient carrying the p.T274M variant was active for only 6 weeks, controlled by anti-epileptic drugs, then in remission without treatment from the age of 1 year (Milh et al., 2013; see also Weckhuysen et al., 2012). It is tempting to speculate that the normalization of the EEG also results from the time-limited alteration of Kv7/M channel function. However, despite this, the patient made almost no motor acquisition and displayed intellectual disability (Milh et al., 2013; Weckhuysen et al., 2012).

Interestingly, *KCNQ<sup>WT/T274</sup>* mice display important cognitive deficits that persist in adulthood (Milh et al., 2020), and we observed that seizures were recorded preferentially in postweaning mice and much less in juvenile mice. Although several questions remain regarding the role of neonatal seizures and early patterns of cortical activity in brain development (Bitzenhofer et al., 2021; Khazipov & Milh, 2018), elucidation of the mechanisms leading to the abolition of effects of the variant on Kv7/M channel function and the reasons why this happens at a particular stage of development represent an important aspect of future studies for an understanding of the pathophysiology of *KCNQ2*-related DEE. In addition, this might have implications for development of therapies with an adapted target and to determine the most appropriate time window during which they should be applied to prevent long-term neurological deficits.

## References

- Abidi, A., Devaux, J. J., Molinari, F., Alcaraz, G., Michon, F. X., Sutura-Sardo, J., Becq, H., Lacoste, C., Altuzarra, C., Afenjar, A., Mignot, C., Doummar, D., Isidor, B., Guyen, S. N., Colin, E., De La Vaissière, S., Haye, D., Trauffer, A., Badens, C., ... Aniksztejn, L. (2015). A recurrent *KCNQ2* pore mutation causing early onset epileptic encephalopathy has a moderate effect on M current but alters subcellular localization of Kv7 channels. *Neurobiology of Disease*, **80**, 80–92.
- Adams, P. R., Brown, D. A., & Constanti, A. (1982). M-currents and other potassium currents in bullfrog sympathetic neurones. *Journal of Physiology*, **330**, 537–572.
- Allen, N. M., Mannion, M., Conroy, J., Lynch, S. A., Shahwan, A., Lynch, B., & King, M. D. (2014). The variable phenotypes of *KCNQ*-related epilepsy. *Epilepsia*, **55**, e99–e105.
- Allen, N. M., Weckhuysen, S., Gorman, K., King, M. D., & Lerche, H. (2020). Genetic potassium channel-associated epilepsies: Clinical review of the Kv family. *European Journal of Paediatric Neurology*, **24**, 105–116.
- Allène, C., Cattani, A., Ackman, J. B., Bonifazi, P., Aniksztejn, L., Ben-Ari, Y., & Cossart, R. (2008). Sequential generation of two distinct synapse-driven network patterns in developing neocortex. *Journal of Neuroscience*, **28**, 12851–12863.
- Battefeld, A., Tran, B. T., Gavrilis, J., Cooper, E. C., & Kole, M. H. P. (2014). Heteromeric Kv7.2/7.3 channels differentially regulate action potential initiation and conduction in neocortical myelinated axons. *Journal of Neuroscience*, **34**, 3719–3732.
- Ben-Ari, Y., Cherubini, E., Corradetti, R., & Gaiarsa, J. L. (1989). Giant synaptic potentials in immature rat CA3 hippocampal neurones. *Journal of Physiology*, **416**, 303–325.
- Ben-Ari, Y., Gaiarsa, J. L., Tyzio, R., & Khazipov, R. (2007). GABA: A pioneer transmitter that excites immature neurons and generates primitive oscillations. *Physiological Reviews*, **87**, 1215–1284.
- Bitzenhofer, S. H., Pöplau, J. A., Chini, M., Marquardt, A., & Hanganu-Opatz, I. L. (2021). A transient developmental increase in prefrontal activity alters network maturation and causes cognitive dysfunction in adult mice. *Neuron*, **109**, 1350–1364.e6.
- Boets, S., Johannesen, K. M., Destree, A., Manti, F., Ramantani, G., Lesca, G., Vercueil, L., Koenig, M. K., Striano, P., Möller, R. S., Cooper, E., & Weckhuysen, S. (2021). Adult phenotype of *KCNQ2* encephalopathy. *Journal of Medical Genetics* 1–8. <https://doi.org/10.1136/jmedgenet-2020-107449>.
- Bonifazi, P., Goldin, M., Picardo, M. A., Jorquera, I., Cattani, A., Bianconi, G., Represa, A., Ben-Ari, Y., & Cossart, R. (2009). GABAergic hub neurons orchestrate synchrony in developing hippocampal networks. *Science*, **326**, 1419–1424.
- Brown, D. A., & Passmore, G. M. (2009). Neural *KCNQ* (Kv7) channels. *British Journal of Pharmacology*, **156**, 1185–1195.
- Carabolana, A., Beguin, S., Pallesi-Pocachard, E., Buhler, E., Pellegrino, C., Arnaud, K., Hubert, P., Oualha, M., Siffroi, J. P., Khantane, S., Couprie, I., Goizet, C., Bernabe Gelot, A., Represa, A., & Cardoso, C. (2012). A glial origin for periventricular nodular heterotopia caused impaired expression of Filamin A. *Human Molecular Genetics*, **21**, 1004–1017.
- Cembrowski, M. S., & Spruston, N. (2019). Heterogeneity within classical cell types is the rule: Lessons from hippocampal pyramidal neurons. *Nature Reviews Neuroscience*, **20**, 193–204.
- Devaux, J. J., Kleopa, K. A., Cooper, E. C., & Scherer, S. S. (2004). *KCNQ2* Is a Nodal K<sup>+</sup> Channel. *Journal of Neuroscience*, **24**, 1236–1244.
- Devaux, J., Dhifallah, S., De Maria, M., Stuart-Lopez, G., Becq, H., Milh, M., Molinari, F., & Aniksztejn, L. (2017). A possible link between *KCNQ2*- and *STXB1*-related encephalopathies: *STXB1* reduces the inhibitory impact of syntaxin-1A on M current. *Epilepsia*, **58**, 2073–2084.
- Dirx, N., Miceli, F., Tagliatela, M., & Weckhuysen, S. (2020). The role of Kv7.2 in neurodevelopment: Insights and gaps in our understanding. *Frontiers in Physiology*, **11**, 570588. <https://doi.org/10.3389/fphys.2020.570588>.
- Fidzinski, P., Korotkova, T., Heidenreich, M., Maier, N., Schuetze, S., Kobler, O., Zuschratter, W., Schmitz, D., Ponomarenko, A., & Jentsch, T. J. (2015). *KCNQ5* K<sup>+</sup> channels control hippocampal synaptic inhibition and fast network oscillations. *Nature Communication*, **6**, 1–13.
- Garaschuk, O., Hanse, E., & Konnerth, A. (1998). Developmental profile and synaptic origin of early network oscillations in the CA1 region of rat neonatal hippocampus. *Journal of Physiology*, **507**, 219–236.
- Garaschuk, O., Linn, J., Eilers, J., & Konnerth, A. (2000). Large-scale oscillatory calcium waves in the immature cortex. *Nature Neuroscience*, **3**, 452–459.
- Ghezzi, F., Corsini, S., & Nistri, A. (2017). Electrophysiological characterization of the M-current in rat hypoglossal motoneurons. *Neuroscience*, **340**, 62–75.
- Greene, D. L., & Hoshi, N. (2017). Modulation of Kv7 channels and excitability in the brain. *Cellular and Molecular Life Sciences*, **74**, 495–508.

- Greene, D. L., Kang, S., & Hoshi, N. (2017). XE991 and linopirdine are state-dependent inhibitors for Kv7/KCNQ channels that favour activated single subunits. *Journal of Pharmacology and Experimental Therapeutics*, **362**, 177–185.
- Gu, N., Vervaeke, K., Hu, H., & Storm, J. F. (2005). Kv7/KCNQ/M and HCN/h, but not KCa2/SK channels, contribute to the somatic medium after-hyperpolarization and excitability control in CA1 hippocampal pyramidal cells. *Journal of Physiology*, **566**, 689–715.
- Guan, D., Higgs, M. H., Horton, L. R., Spain, W. J., & Foehring, R. C. (2011). Contributions of Kv7-mediated potassium current to sub- and suprathreshold responses of rat layer II/III neocortical pyramidal neurons. *Journal of Neurophysiology*, **106**, 1722–1733.
- Grigorov, A., Moskalyuk, A., Kravchenko, M., Veselovsky, N., Verkhratsky, A., & Fedulova, S. (2014). Kv7 potassium channel subunits and M currents in cultured hippocampal interneurons. *Pflügers Archiv – European Journal of Physiology*, **466**, 1747–1758.
- Griguoli, M., & Cherubini, E. (2017). Early correlated network activity in the hippocampus: Its putative role in shaping neuronal circuits. *Frontiers in Cellular Neuroscience*, **11**, 1–11.
- Hönigsperger, C., Marosi, M., Murphy, R., & Storm, J. F. (2015). Dorsoventral differences in Kv7/M-current and its impact on resonance, temporal summation and excitability in rat hippocampal pyramidal cells. *Journal of Physiology*, **593**, 1551–1580.
- Hou, B., Varghese, N., Soh, H., Santaniello, S., & Tzingounis, A. V. (2021). Loss of *kcnq2* or *kcnq3* leads to multifocal time-varying activity in the neonatal forebrain *ex vivo*. *eNeuro*, **8**, 1–28.
- Hu, H., Vervaeke, K., & Storm, J. F. (2002). Two forms of electrical resonance at theta frequencies, generated by M-current, h-current and persistent Na<sup>+</sup> current in rat hippocampal pyramidal cells. *Journal of Physiology*, **545**, 783–805.
- Hu, H., Vervaeke, K., & Storm, J. F. (2007). M-channels (Kv7/KCNQ Channels) that regulate synaptic integration, excitability, and spike pattern of CA1 pyramidal cells are located in the perisomatic region. *Journal of Neuroscience*, **27**, 1853–1867.
- Hu, W., & Bean, B. P. (2018). Differential control of axonal and somatic resting potential by voltage-dependent conductances in cortical layer 5 pyramidal neurons. *Neuron*, **97**, 1315–1326.e3.
- Huang, H., & Trussell, L. O. (2011). KCNQ5 channels control resting properties and release probability of a synapse. *Nature Neuroscience*, **14**, 840–847.
- Jentsch, T. J. (2000). Neuronal KCNQ potassium channels: Physiology and role in disease. *Nature Reviews Neuroscience*, **1**, 21–30.
- Jiang, X., Shen, S., Cadwell, C. R., Berens, P., Sinz, F., Ecker, A. S., Patel, S., & Tolias, A. S. (2015). Principles of connectivity among morphologically defined cell types in adult neocortex. *Science*, **350**, aac9462; <https://doi.org/10.1126/science.aac9462>.
- Kato, M., Yamagata, T., Kubota, M., Arai, H., Yamashita, S., Nakagawa, T., Fujii, T., Sugai, K., Imai, K., Uster, T., Chitayat, D., Weiss, S., Kashii, H., Kusano, R., Matsumoto, A., Nakamura, K., Oyazato, Y., Maeno, M., Nishiyama, K., ... Saitsu, H. (2013). Clinical spectrum of early onset epileptic encephalopathies caused by KCNQ2 mutation. *Epilepsia*, **54**, 1282–1287.
- Kim, K. S., Kobayashi, M., Takamatsu, K., & Tzingounis, A. V. (2012). Hippocalcin and KCNQ channels contribute to the kinetics of the slow afterhyperpolarization. *Biophysical Journal*, **103**, 2446–2454.
- Kim, K. S., Patel, J., Zhang, J., Soh, H., Rhodes, J. S., Tzingounis, A. V., & Chung, H. J. (2020). Heterozygous loss of epilepsy gene KCNQ2 alters social, repetitive and exploratory behaviors. *Genes, Brain, and Behavior*, **19**, e12599.
- Kim, E. C., Zhang, J., Tang, A. Y., Bolton, E. C., Rhodes, J. S., Christian-Hinman, C. A., & Chung, H. J. (2021). Spontaneous seizure and memory loss in mice expressing an epileptic encephalopathy variant in. *PNAS*, **118**, e2021265118.
- Khalilov, I., Minlebaev, M., Mukhtarov, M., & Khazipov, R. (2015). Dynamic changes from depolarizing to hyperpolarizing GABAergic actions during giant depolarizing potentials in the neonatal rat hippocampus. *Journal of Neuroscience*, **35**, 12635–12642.
- Khazipov, R., & Milh, M. (2018). Early patterns of activity in the developing cortex: Focus on the sensorimotor system. *Seminars in Cell & Developmental Biology*, **76**, 120–129.
- Landmesser, L. T., & O'Donovan, M. J. (1984). Activation patterns of embryonic chick hind limb muscles recorded *in ovo* and in an isolated spinal cord preparation. *Journal of Physiology*, **347**, 189–204.
- Lawrence, J. J., Saraga, F., Churchill, J. F., Statland, J. M., Travis, K. E., Skinner, F. K., & McBain, C. J. (2006). Somatodendritic Kv7/KCNQ/M channels control interspike interval in hippocampal interneurons. *Journal of Neuroscience*, **26**, 12325–12338.
- Manville, R. W., Neverisky, D. L., & Abbott, G. W. (2017). SMI1 modifies KCNQ channel function and pharmacology by physical interaction with the pore. *Biophysical Journal*, **113**, 613–626.
- Marguet, S. L., Le-Schulte, V. T. Q., Merseburg, A., Neu, A., Eichler, R., Jakovcevski, I., Ivanov, A., Hanganu-Opatz, I. L., Bernard, C., Morellini, F., & Isbrandt, D. (2015). Treatment during a vulnerable developmental period rescues a genetic epilepsy. *Nature Medicine*, **21**, 1436–1444.
- Marissal, T., Bonifazi, P., Picardo, M. A., Nardou, R., Petit, L. F., Baude, A., Fishell, G. J., Ben-Ari, Y., & Cossart, R. (2012). Pioneer glutamatergic cells develop into a morpho-functionally distinct population in the juvenile CA3 hippocampus. *Nature Communication*, **3**, 1316.
- Martinello, K., Giacalone, E., Migliore, M., Brown, D. A., & Shah, M. M. (2019). The subthreshold-active KV7 current regulates neurotransmission by limiting spike-induced Ca<sup>2+</sup> influx in hippocampal mossy fiber synaptic terminals. *Communications Biology*, **2**, 145. <https://doi.org/10.1038/s42003-019-0408-4>.

- McTague, A., Howell, K. B., Cross, J. H., Kurian, M. A., & Scheffer, I. E. (2016). The genetic landscape of the epileptic encephalopathies of infancy and childhood. *Lancet Neurology*, **15**, 304–316.
- Meister, M., Wong, R. O., Baylor, D. A., & Shatz, C. J. (1991). Synchronous bursts of action potentials in ganglion cells of the developing mammalian retina. *Science*, **252**, 939–943.
- Miceli, F., Virginia, M., Ambrosino, P., Barrese, V., & Migliore, M. (2013). Genotype–phenotype correlations in neonatal epilepsies caused by mutations in the voltage sensor of Kv7.2 potassium channel subunits. *PNAS*, **110**, 4386–4391.
- Milh, M., Boutry-Kryza, N., Sutura-Sardo, J., Mignot, C., Auvin, S., Lacoste, C., Villeneuve, N., Roubertie, A., Heron, B., Carneiro, M., Kaminska, A., Altuzarra, C., Blanchard, G., Ville, D., Barthez, M. A., Heron, D., Gras, D., Afenjar, A., Dorison, N., ... Villard, L. (2013). Similar early characteristics but variable neurological outcome of patients with a de novo mutation of KCNQ2. *Orphanet Journal of Rare Diseases*, **8**, 0–7.
- Milh, M., Lacoste, C., Cacciagli, P., Abidi, A., Sutura-Sardo, J., Tzelepis, I., Colin, E., Badens, C., Afenjar, A., Coeslier, A. D., Dailland, T., Lesca, G., Philip, N., & Villard, L. (2015). Variable clinical expression in patients with mosaicism for KCNQ2 mutations. *Am J Med Genet Part A*, **167**, 2314–2318.
- Milh, M., Roubertoux, P., Biba, N., Chavany, J., Spiga Ghata, A., Fulachier, C., Collins, S. C., Wagner, C., Roux, J. C., Yalcin, B., Félix, M. S., Molinari, F., Lenck-Santini, P. P., & Villard, L. (2020). A knock-in mouse model for KCNQ2-related epileptic encephalopathy displays spontaneous generalized seizures and cognitive impairment. *Epilepsia*, **61**, 868–878.
- Mizuseki, K., Diba, K., Pastalkova, E., & Buzsáki, G. (2011). Hippocampal CA1 pyramidal cells form functionally distinct sublayers. *Nature Neuroscience*, **14**, 1174–1181.
- Módl, L., Sousa, V. H., Malvache, A., Tressard, T., Baude, A., & Cossart, R. (2017). Spatial embryonic origin delineates gabaergic hub neurons driving network dynamics in the developing entorhinal cortex. *Cerebral Cortex*, **27**, 4649–4661.
- Niday, Z., Hawkins, V. E., Soh, H., Mulkey, D. K., & Tzingounis, A. V. (2017). Epilepsy-associated KCNQ2 channels regulate multiple intrinsic properties of layer 2/3 pyramidal neurons. *Journal of Neuroscience*, **37**, 576–586.
- Nieto-Gonzalez, J. L., & Jensen, K. (2013). BDNF depresses excitability of parvalbumin-positive interneurons through an M-Like current in rat dentate gyrus. *Plos One*, **8**, e67318.
- Orhan, G., Bock, M., Schepers, D., Ilna, E. I., Reichel, S. N., Löffler, H., Jezutkovic, N., Weckhuysen, S., Mandelstam, S., Suls, A., Danker, T., Guenther, E., Scheffer, I. E., De Jonghe, P., Lerche, H., & Maljevic, S. (2014). Dominant-negative effects of KCNQ2 mutations are associated with epileptic encephalopathy. *Annals of Neurology*, **75**, 382–394.
- Peters, H. C., Hu, H., Pongs, O., Storm, J. F., & Isbrandt, D. (2005). Conditional transgenic suppression of M channels in mouse brain reveals functions in neuronal excitability, resonance and behavior. *Nature Neuroscience*, **8**, 51–60.
- Petit, L. F., Jalabert, M., Buhler, E., Malvache, A., Peret, A., Chauvin, Y., Watrin, F., Represa, A., & Manent, J. B. (2014). Normotopic cortex is the major contributor to epilepsy in experimental double cortex. *Annals of Neurology*, **76**, 428–442.
- Picardo, M. A., Guigue, P., Bonifazi, P., Batista-Brito, R., Allene, C., Ribas, A., Fishell, G., Baude, A., & Cossart, R. (2011). Pioneer GABA cells comprise a subpopulation of hub neurons in the developing hippocampus. *Neuron*, **71**, 695–709.
- Rahmati, N., Normoyle, K. P., Glykys, J., Dzhala, V. I., Lillis, K. P., Kahle, K. T., Raiyyani, R., Jacob, T., & Staley, K. J. (2021). Unique actions of GABA arising from cytoplasmic chloride microdomains. *Journal of Neuroscience*, **41**, 4957–4975.
- Safulina, V. F., Zacchi, P., Tagliatalata, M., Yaari, Y., & Cherubini, E. (2008). Low expression of Kv7/M channels facilitates intrinsic and network bursting in the developing rat hippocampus. *Journal of Physiology*, **586**, 5437–5453.
- Schroeder, B. C., Hechenberger, M., Weinreich, F., Kubisch, C., & Jentsch, T. J. (2000). KCNQ5, a novel potassium channel broadly expressed in brain, mediates M-type currents. *Journal of Biological Chemistry*, **275**, 24089–24095.
- Shah, M. M., Migliore, M., Valencia, I., Cooper, E. C., & Brown, D. A. (2008). Functional significance of axonal Kv7 channels in hippocampal pyramidal neurons. *PNAS*, **105**, 7869–7874.
- Shah, M. M., Migliore, M., & Brown, D. A. (2011). Differential effects of Kv7 (M-) channels on synaptic integration in distinct subcellular compartments of rat hippocampal pyramidal neurons. *Journal of Physiology*, **589**, 6029–6038.
- Simkin, D., Marshall, K. A., Vanoye, C. G., Desai, R. R., Bustos, B. I., Piyevsky, B. N., Ortega, J. A., Forrest, M., Robertson, G. L., Penzes, P., Laux, L. C., Lubbe, S. J., Millichap, J. J., Jr, A. L. G., & Kiskinis, E. (2021). Dyshomeostatic modulation of Ca<sup>2+</sup>-activated K<sup>+</sup> channels in a human neuronal model of KCNQ2 encephalopathy. *Elife*, **10**:e644341.
- Soh, H., Pant, R., LoTurco, J. J., & Tzingounis, A. V. (2014). Conditional deletions of epilepsy-associated KCNQ2 and KCNQ3 channels from cerebral cortex cause differential effects on neuronal excitability. *Journal of Neuroscience*, **34**, 5311–5321.
- Soh, H., Park, S., Ryan, K., Springer, K., Maheshwari, A., & Tzingounis, A. V. (2018). Deletion of KCNQ2/3 potassium channels from PV+ interneurons leads to homeostatic potentiation of excitatory transmission. *Elife*, **7**, e386171.
- Storm, J. F. (1990). Understanding the brain through the hippocampus the hippocampal region as a model for studying brain structure and function. *Progress in Brain Research*, **83**, 161–187.
- Tanaka, K., Watase, K., Manabe, T., Yamada, K., Watanabe, M., Takahashi, K., Iwama, H., Nishikawa, T., Ichihara, N., Kikuchi, T., Okuyama, S., Kawashima, N., Hori, S., Takimoto, M., & Wada, K. (1997). Epilepsy and exacerbation of brain injury in mice lacking the glutamate transporter GLT-1. *Science*, **276**, 1699–1702.
- Tyzio, R., Ivanov, A., Bernard, C., Holmes, G. L., Ben-Ari, Y., & Khazipov, R. (2003). Membrane potential of CA3 hippocampal pyramidal cells during postnatal development. *Journal of Neurophysiology*, **90**, 2964–2972.

- Zzingounis, A. V., Heidenreich, M., Kharkovets, T., Spitzmaul, G., Jensen, H. S., Nicoll, R. A., & Jentsch, T. J. (2010). The KCNQ5 potassium channel mediates a component of the afterhyperpolarization current in mouse hippocampus. *PNAS*, **107**, 10232–10237.
- Uchida, T., Lossin, C., Ihara, Y., Deshimaru, M., Yanagawa, Y., Koyama, S., & Hirose, S. (2017). Abnormal  $\gamma$ -aminobutyric acid neurotransmission in a Kcnq2 model of early onset epilepsy. *Epilepsia*, **58**, 1430–1439.
- Verneuil, J., Brocard, C., Trouplin, V., Villard, L., Peyronnet-Roux, J., & Brocard, F. (2020). The M-current works in tandem with the persistent sodium current to set the speed of locomotion. *Plos Biology*, **18**, e3000738.
- Vervaeke, K., Gu, N., Agdestein, C., Hu, H., & Storm, J. F. (2006). Kv7/KCNQ/M-channels in rat glutamatergic hippocampal axons and their role in regulation of excitability and transmitter release. *Journal of Physiology*, **576**, 235–256.
- Wang, H. S., Pan, Z., Shi, W., Brown, B. S., Wymore, R. S., Cohen, I. S., Dixon, J. E., & McKinnon, D. (1998). KCNQ2 and KCNQ3 potassium channel subunits: Molecular correlates of the M-channel. *Science*, **282**, 1890–1893.
- Watanabe, H., Nagata, E., Kosakai, A., Nakamura, M., Yokoyama, M., Tanaka, K., & Sasai, H. (2000). Disruption of the epilepsy KCNQ2 gene results in neuronal hyperexcitability. *Journal of Neurochemistry*, **75**, 28–33.
- Weckhuysen, S., Mandelstam, S., Suls, A., Audenaert, D., Deconinck, T., Claes, L. R. F., Deprez, L., Smets, K., Hristova, D., Yordanova, I., Jordanova, A., Ceulemans, B., Jansen, A., Hasaerts, D., Roelens, F., Lagae, L., Yendle, S., Stanley, T., Heron, S. E., & Mulley, J. C. (2012). KCNQ2 encephalopathy: Emerging phenotype of a neonatal epileptic encephalopathy. *Annals of Neurology*, **71**, 15–25.
- White, A., Williams, P. A., Ferraro, D. J., Clark, S., Kadam, S. D., Dudek, F. E., & Staley, K. J. (2006). Efficient unsupervised algorithms for the detection of seizures in continuous EEG recordings from rats after brain injury. *Journal of Neuroscience Methods*, **152**, 255–266.
- Yue, C., & Yaari, Y. (2006). Axo-somatic and apical dendritic Kv7/M channels differentially regulate the intrinsic excitability of adult rat CA1 pyramidal cells. *Journal of Neurophysiology*, **95**, 3480–3495.
- ex vivo* electrophysiological recordings and contributed to data analysis. M.K. performed histological analysis after EEG recordings. E.P. and A.M. performed western blot experiments. S.G. and S.S. performed statistical analysis. L.V. provided the knock-in mice. M.M. contributed to *in vivo* data analysis. P.-P.L.S. designed and supervised *in vivo* electrophysiological recordings, performed the program for *in vivo* data analysis and analysed *in vivo* data. L.A. designed the work, performed *ex vivo* electrophysiological recordings, analysed data and wrote the manuscript. All authors have read and approved the final version of this manuscript and agree to be accountable for all aspects of the work in ensuring that questions related to the accuracy or integrity of any part of the work are appropriately investigated and resolved. All persons designated as authors qualify for authorship, and all those who qualify for authorship are listed.

## Funding

This work was supported by INSERM (Institut National de la Santé et de la Recherche Médicale), by the Agence National pour la Recherche (ANR 19-CE17-0018-02, IMprove), by the Ministère de l'Enseignement Supérieur, de la Recherche et de l'Innovation (N.B.M.) and by the Ligue Française contre l'Epilepsie (N.B.M.).

## Acknowledgements

We would also like to thank Francesca Bader for genotyping the mice (PBMC at INMED) and technicians working at the animal facility at INMED for excellent technical support. Finally, we thank Dr Jérôme Epsztein for his constructive remarks on the manuscript and Robin Dard for his precious help.

## Keywords

epileptic encephalopathy, Kv7 channels, M current, neocortex, neuronal excitability, pyramidal neurons

## Additional information

### Data availability statement

Numerical values used to construct graphs can be found in the summary statistical document. They are found in the figures when constructing boxplots.

### Competing interests

The authors declare no competing interests.

### Author contributions

N.B.M. performed *ex vivo* and *in vivo* electrophysiological recordings and contributed to data analysis. H.B. performed

## Supporting information

Additional supporting information can be found online in the Supporting Information section at the end of the HTML view of the article. Supporting information files available:

### Statistical Summary Document

### Peer Review History

**Supplemental Video 1:** Video-EEG monitoring of a generalized seizure in a *KCNQ2*<sup>WT/T274M</sup> mice.

**Supplemental Video 2:** Video-EEG monitoring of a partial seizure with spike and wave activities in the right hippocampus and without visible behavioural manifestation in a *KCNQ2*<sup>WT/T274M</sup>.

### Translational perspective

Early-onset developmental encephalopathies with epilepsy (DEEs) are particularly challenging neurological conditions for clinicians because they combine severe neurodevelopmental disorders with intractable epilepsy. The majority of early-onset DEEs are caused by genetic alterations of the *KCNQ2* gene. To study the mechanisms of epilepsy, neurodevelopmental deficits and their interdependence, we recently generated a mouse model carrying the pathogenic p.T274M mutation in *KCNQ2*. These mice display remitting epileptic seizures and persistent cognitive deficits, which are characteristic features of *KCNQ2*-related DEE. Biba-Maazou et al. have now analyzed the electrophysiological consequences of the variant in developing motor cortical pyramidal cells in this KI mouse. The authors show that the M current is decreased, that pyramidal cells are hyperexcitable, and that GABA-mediated network activities are increased. Interestingly, as with seizures, these effects are time limited; they are observed only in neonatal and postweaning stages, but not later. Altogether, these results suggest that a self-correction mechanism takes place that might explain the remission of seizures observed in this model. However, such normalization might not be sufficient to prevent cognitive deficits. This reinforces the hypothesis of a critical period, during which Kv7 channels play a crucial role in brain development. This has important therapeutic consequences because it suggests that treatment initiated after this period would not be sufficient to treat the cognitive deficits in these DEEs. Identification of this critical period will therefore be essential to improve the cognitive prognosis of early-onset DEEs effectively.